Diurnal Variability of the Marine Boundary Layer during ASTEX

PAUL E. CIESIELSKI, WAYNE H. SCHUBERT, AND RICHARD H. JOHNSON

Department of Atmospheric Science, Colorado State University, Fort Collins, Colorado

(Manuscript received 20 June 2000, in final form 31 January 2001)

ABSTRACT

The diurnal cycle of the marine boundary layer over the Atlantic Stratocumulus Transition Experiment (ASTEX) domain is examined during a two-week period of June 1992 in several fields, including: fractional low cloudiness, various parameters that enter into the heat and moisture budgets (e.g., temperature, water vapor mixing ratio, vertical motion), the budgets themselves, radiative heating, and the vertical eddy flux of moist static energy. Results show fractional low cloudiness varies over this region from a maximum of 54% in the predawn hours to a minimum of 39% in the midafternoon. These changes in low cloudiness are accompanied by an opposite trend in the boundary layer moisture, which shows a predawn drying and an afternoon moistening. Large-scale vertical motion also varies diurnally with a peak amplitude of 0.12 cm s^{-1} at 1.8 km, which is a ~20% variation from the mean subsidence rate. Cloud-radiative processes play an important role in determining the diurnal characteristics of the vertical eddy flux of moist static energy, with a peak amplitude in the cloud layer at 1.2 km and a variation at this level from 24 W m^{-2} at 1300 LST to 100 W m^{-2} at 0400 LST. These diurnal changes suggest that the early morning peak in eddy flux results in a drying of the subcloud layer as moisture transport into the cloud layer is enhanced, leading to the observed low-cloud maximum. In contrast, during the daylight hours, solar heating within the cloud leads to a well-mixed cloud layer, a stabilizing of the subcloud layer with respect to the cloud layer, a decoupling of the cloud and subcloud layers, and ultimately, a thinning or reduction of the low clouds.

Comparison of the diurnal cycle of summertime low-level divergence and vertical motion from this study with earlier published results from other regions in the North Atlantic shows a complex diurnal pattern with alternating phase in adjacent latitude belts across this region. The sense of these phase changes suggests that the northern branch of the Hadley circulation from roughly 5°N to 25°N over the eastern Atlantic is pulsing diurnally with enhanced mass flow during the early morning hours.

1. Introduction

Over the past 30 years several field campaigns conducted over the North Atlantic region have focused on the interaction of convection with its large-scale environment. Recently, Ciesielski et al. (1999, hereafter referred to as CSJ99) examined the mean and transient characteristics of large-scale heat and moisture budgets for a 2-week period over the Atlantic Stratocumulus Transition Experiment (ASTEX) domain. Consistent with earlier budget studies of the Atlantic trades (Augstein et al. 1973; Holland and Rasmusson 1973; Nitta and Esbensen 1974b), the mean budget profiles over ASTEX revealed a significant apparent cooling and moistening near the inversion layer. These results suggest that the trade inversion layer over these regions is maintained as a balance between radiative and small-scale convective effects, which tend to cool and moisten the inversion layer, and large-scale subsidence, which warms and dries the layer. In addition to their presentation of mean budget profiles, CSJ99 observed that the atmospheric state during ASTEX was not that of a steady, invariant environment, but rather cloudiness and large-scale fields were strongly modulated on synoptic and shorter timescales. On the synoptic timescale, CSJ99 attributed much of the observed variability to fluctuations in the subsidence rate associated with changes in the strength and position of the Azores high and the passage of fronts.

The present paper further examines the temporal variability over the ASTEX domain, with a focus on the diurnal timescale. Satellite evidence for diurnal variability in the ASTEX region was presented by Rozendaal et al. (1995), who showed diurnal fluctuations in low-level stratiform cloud amounts with peak amplitudes greater than 10% (or a 25% variation from the mean) centered about 500 km off the northwest coast of Africa. Using ASTEX datasets, Miller and Albrecht (1995) and Rogers et al. (1995) describe dramatic diurnal changes in mesoscale cloud and boundary layer structures during a single 24-h period, while Bretherton et al. (1995) and Betts et al. (1995) have documented substantial diurnal variations in fractional cloudiness

Corresponding author address: Paul E. Ciesielski, Department of Atmospheric Science, Colorado State University, Fort Collins, CO 80523.
E-mail: paulc@tornado.atmos.colostate.edu

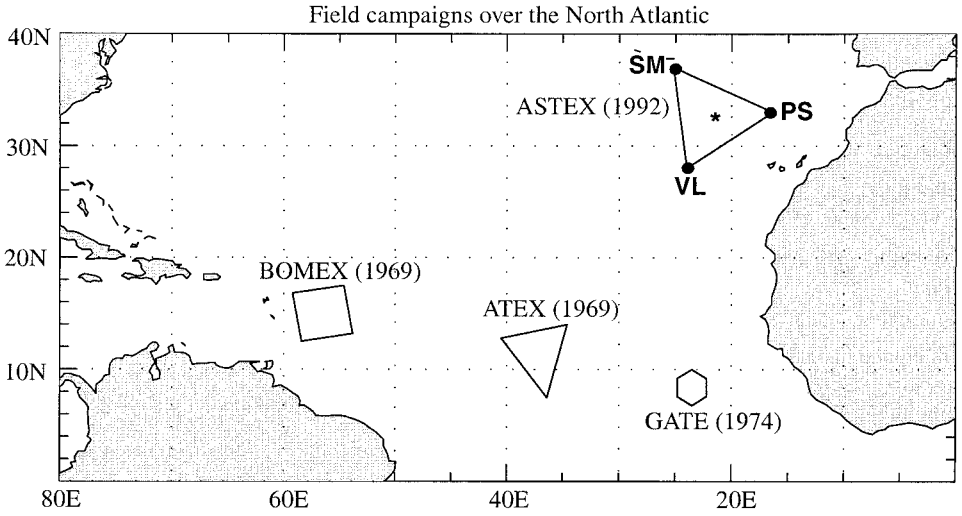

FIG. 1. Location of field campaigns over the North Atlantic: ATEX conducted in Feb 1969, BOMEX conducted from May to Jul 1969, GATE conducted from Jun to Sep 1974, and ASTEX conducted during Jun 1992. ATEX data was from a ship array that drifted with the trade wind flow. The location of the ATEX polygon shown here represents its position on 10 Feb 1969. The vertices of the polygons indicate the location of sounding sites during these experiments. The asterisk near the center of the ASTEX triangle shows the position of the buoy described in the text.

and boundary layer stability. Because of the high temporal resolution of the data collected in ASTEX (from 1-min cloud data to 3-h atmospheric soundings), we have an unprecedented opportunity to study diurnal variations in a unique region where low-level air flowing equatorward within the Hadley circulation transitions between a stratocumulus and a trade cumulus regime.

Because of the importance of tropical convection to global climate, numerous studies have documented the diurnal variation of convection and related fields over the tropical oceans. While unorganized deep convection over the continents typically peaks in the late afternoon or early evening and is linked to maximum surface heating, deep convective activity over the tropical oceans generally maximizes in the early morning (Gray and Jacobson 1977; Murakami 1983; Hendon and Woodberry 1993). The early morning maximum in deep convection over the oceans is associated with a substantial diurnal variation in the mass circulation. Examining the diurnal cycle of divergence and vertical motion in regions of deep convection in the western Pacific and the Atlantic, McBride and Gray (1980) found that the mass convergence below 850 hPa peaks around 0730 LST. Based on surface wind analyses from the Tropical Atmosphere–Ocean moored buoy array over the Pacific, Deser and Smith (1998) presented compelling evidence for a diurnal modulation of the Hadley circulation, which links an early morning rainfall maximum in the intertropical convergence zone (ITCZ) near 10°N to a diurnal maximum in surface divergence at 0700 LST over the equatorial Pacific. Over this region, Deser and Smith found the diurnal amplitude of the zonal mean surface divergence to be 0.45×10^{-6} s^{-1}, which is a 45% variation from the daily mean.

Over the North Atlantic, detailed diurnal analyses of the marine boundary layer have been restricted to limited regions where field campaigns have enhanced observational networks. Figure 1 shows the location of four field experiments that were conducted over the North Atlantic: two experiments that were located within the trade wind regime—the Atlantic Trade-Wind Experiment (ATEX) and the Barbados Oceanographic and Meteorological Experiment (BOMEX); the GARP (Global Atmospheric Research Program) Atlantic Tropical Experiment (GATE), which was situated within the Atlantic ITCZ; and, finally, ASTEX, which is of primary interest to this study. Although sea surface temperatures (SSTs) in the subtropical North Atlantic exhibit a very limited diurnal range (e.g., Delnore 1972), significant diurnal variability has been found in the boundary layer and associated cloud fields. Analysis by Brill and Albrecht (1982) for a 6-day period of undisturbed trade flow in ATEX revealed a substantial diurnal cycle in the cloud fraction and divergence fields. For example, low-level divergence over ATEX peaked at 0700 LST with a diurnal amplitude of 1.0×10^{-6} s^{-1} representing a 25% variation from the daily mean. Using BOMEX data for an 8-day undisturbed period, Nitta and Esbensen (1974a) also found a morning (0800 LST) low-level divergence maximum with an amplitude of 1.5×10^{-6} s^{-1} (about a 50% variation from the mean). In contrast, GATE analysis reveals a nighttime diurnal maximum in low-level divergence that peaks around 2230 LST. One of the primary objectives in this study is to geograph-

TABLE 1. Statistics for various fields (see text for definition of symbols) for 2-week period in Jun 1992. Last column is a measure of the significance of the diurnal signal relative to the background variability. Location of the buoy is shown in Fig. 1. The horizontal location ''ASTEX'' refers to an average over the ASTEX triangle. Statistics for fields that are a function of height were averaged over a 0.2-km layer centered at the level where the diurnal amplitude of that field was a maximum in the vertical. The values in parentheses represent the diurnal amplitudes for the idealized computation with corrected humidity described in the text and shown in Fig. 10.

Field	Temporal resolution	Observation location		Mean	Standard deviation (SD)	Diurnal amplitude (DA)	DA/SD (percent)
		Vertical	Horizontal				
SST (°C)	1-h	Surface	Buoy	19.8	0.3	0.15	50
T_0 (°C)	1-h	Surface	Buoy	18.8	0.6	0.23	38
q_0 (g kg^{-1})	1-h	Surface	Buoy	10.1	1.1	0.06	6
q^* (g kg^{-1})	1-h	Surface	Buoy	14.2	0.3	0.13	43
u_0 (m s^{-1})	1-h	Surface	Buoy	−1.5	1.5	0.27	18
v_0 (m s^{-1})	1-h	Surface	Buoy	−5.0	1.8	0.10	6
$\lvert\mathbf{v}_0\rvert$ (m s^{-1})	1-h	Surface	Buoy	5.4	1.8	0.10	7
S_0 (W m^{-2})	1-h	Surface	Buoy	8.0	4.2	0.9	21
LE_0 (W m^{-2})	1-h	Surface	Buoy	85.0	30.4	3.6	11
σ (%)	1-h		SM	57.9	28.3	6.5	23
σ (%)	1-h		PS	46.9	24.3	7.5	31
σ (%)	1-h		VL	44.1	28.0	13.0	46
σ (%)	1-h		ASTEX	46.4	20.0	7.2	40
z_{ct} (m)	3-h	I_b	SM	1253.0	454.0	12.0	3
z_{ct} (m)	3-h	I_b	PS	1579.0	412.0	90.0	23
z_{ct} (m)	3-h	I_b	VL	1533.0	329.0	30.0	9
z_{cb} (m)	1-h		PS	884.0	262.0	56.0	21
PW_S (mm)	3-h		PS	21.3	2.8	0.80	28
PW_r (mm)	1-h		PS	21.6	3.6	0.43	12
LWP (mm)	1-h		PS	0.83	1.6	0.21	13
θ (°K)	3-h	1.1–1.2 km	ASTEX	293.0	1.5	0.45	30
q (g kg^{-1})	3-h	0.8–1.0 km	ASTEX	7.9	1.0	0.32	32
ζ (10^{-6} s^{-1})	3-h	0.9–1.1 km	ASTEX	−10.2	6.8	1.4	21
δ (10^{-6} s^{-1})	3-h	1.4–1.6 km	ASTEX	3.9	4.9	1.2	25
w (cm s^{-1})	3-h	1.7–1.9 km	ASTEX	−0.6	0.41	0.12	29
ω (mb h^{-1})	3-h	1.7–1.9 km	ASTEX	2.5	1.8	0.45	25
Q_1 (K day^{-1})	3-h	1.4–1.6 km	ASTEX	−3.4	6.0	2.8	47
Q_2 (K day^{-1})	3-h	0.9–1.1 km	ASTEX	−3.5	8.7	5.2 (3.5)	60
Q_R (K day^{-1})	3-h	1.3–1.5 km	ASTEX	−3.1	8.7	3.2 (12.2)	37
$\rho w'h'$ (W m^{-2})	3-h	1.1–1.3 km	ASTEX	64.4	38.1	30.0 (38.0)	78

ically extend documentation of the diurnal cycle beyond the domains of these previous experiments by considering its characteristics over the ASTEX region.

Recently, Dai and Deser (1999) examined the diurnal and semidiurnal variations in surface divergence over the globe from 50°S to 70°N using 20 years of 3-hourly wind observations from land stations and the Comprehensive Ocean–Atmosphere Data Set. Over the North Atlantic, their diurnal analysis reveals zonally coherent phase structures in surface divergence with alternating phase in adjacent latitude belts. Despite significantly different averaging periods, their phase analysis of low-level divergence agrees reasonably well with results from the North Atlantic field experiments cited above. An overview and comparison of these diurnal phase results is presented in section 4 to provide a more complete description of diurnal variability over the North Atlantic.

A variety of mechanisms have been considered to explain diurnal variability of the boundary layer and associated cloud fields over oceanic regions. Over the ocean where surface forcing is weak, proposed mechanisms used to explain the observed diurnal cycle of deep convection include differences in tropospheric radiative cooling rates between clear and cloudy regions (Gray and Jacobson 1977) and stability changes due to direct radiation–convection interactions (Randall et al. 1991). In the trade wind boundary layer, Brill and Albrecht (1982) used observations and model results to show that diurnal variations are primarily a result of radiative forcing and secondarily a result of diurnal fluctuations in large-scale divergence. Using predominately observational analyses, we will show that radiative effects within the cloud layer play a prominent role in determining diurnal variability in the marine boundary layer of ASTEX. Nitta and Esbensen (1974a) suggested that the diurnal low-level flow field over BOMEX was influenced by land–sea heating contrasts from the South American continent. Using a simplified version of a mesoscale model, we explore the possible influence of land–sea circulations on the flow over ASTEX.

The main purpose of this paper is to document the diurnal variability in the marine boundary layer and associated cloud fields during ASTEX. Section 2 describes the data and analysis procedures. Using a variety of observations and model-generated radiative heating profiles, section 3 describes the characteristics of the diurnal cycle of boundary layer and cloud-layer prop-

erties over ASTEX. To provide a larger-scale context for the ASTEX results, section 4 examines the diurnal variability of divergence and vertical motion in adjacent regions of the North Atlantic. A summary of the ASTEX diurnal results and some concluding remarks are offered in section 5.

2. Data and analysis procedure

During a 2-week period in early June 1992, three sounding sites within the ASTEX domain launched high-resolution (~3 s) atmospheric soundings, typically at 3-h intervals. These sites, located at the vertices of the ASTEX triangle, which is shown in Fig. 1, include the R/V *Valdivia* (VL) positioned at 28.0°N, 24.0°W, along with the island stations of Porto Santo (PS; 33.1°N, 16.4°W) and Santa Maria (SM; 37.0°N, 25.2°W). The sonde sampling frequency of eight times per day enabled us to examine diurnal variability of kinematic and thermodynamic fields in the sounding data. The processing and quality control of the original raw sounding data into a 25-m interval dataset is discussed in CSJ99.

Upper-air observations at SM and VL were made using a Vaisala model RS-80 radiosonde system, while at PS a VIZ system was used. Vaisala systems measure temperature and humidity based on capacitance sensors, as opposed to resistive sensors used on VIZ systems. Errors and difficulties in measuring humidity with these systems have been reported in several recent publications (e.g., Garand et al. 1992; Cole 1993; Wade 1995). In their analyses of VL sonde data from ASTEX, Betts et al. (1995) excluded humidity data at 1000 LST and 1300 LST due to excessive boundary layer drying at these times. They attribute at least part of this daytime drying to solar heating of the humicap sensor on the Vaisala sondes. Similar humidity problems on Vaisala systems used in the Tropical Ocean Global Atmosphere Coupled Ocean–Atmosphere Response Experiment (TOGA COARE) were documented by Cole (1993). Despite the different types of sonde systems used in ASTEX, excessive daytime drying (as noted by Betts et al. at VL) was also observed in the sonde data at the other sites. Additional details of these humidity errors and a simple procedure to correct them for use in the budget analyses are described in the following section.

Area-averaged vorticity and divergence are computed over the ASTEX triangle using standard line integral techniques. Using the computations of divergence, vertical motion is evaluated by integration of the anelastic continuity equation. Because of the questionable quality of the upper-level sounding winds, the divergence and vertical motion fields in CSJ99 were adjusted using the 600-hPa vertical motion analysis from a special European Centre for Medium-Range Weather Forecasts (ECMWF) dataset prepared for the ASTEX period. However, Betts et al. (1995) have shown that on a timescale of less than a day the ECMWF vertical motion analyses during ASTEX were quite noisy due to model spinup every 6 h. Thus to isolate the diurnal signal within the sounding data, no adjustments are made in this present study.

The apparent heat source Q_1 and the apparent moisture sink Q_2 (Yanai et al. 1973) are computed from

$$Q_1 = c_p\left(\frac{\overline{p}}{p_0}\right)^{\kappa}\left(\frac{\partial\overline{\theta}}{\partial t} + \overline{\nabla\cdot(\mathbf{v}\theta)} + \frac{\partial(\rho\overline{w}\,\overline{\theta})}{\rho\partial z}\right), \quad (1)$$

$$Q_2 = -L\left(\frac{\partial\overline{q}}{\partial t} + \overline{\nabla\cdot(\mathbf{v}q)} + \frac{\partial(\rho\overline{w}\,\overline{q})}{\rho\partial z}\right), \quad (2)$$

where θ is potential temperature, q is the mixing ratio of water vapor, $\mathbf{v}$ is horizontal wind, w is vertical motion, p is density, c_p is the specific heat of dry air at constant pressure, L the latent heat of condensation, $p_0 = 1000$ hPa the constant reference pressure, and the overbar refers to a horizontal average over the ASTEX triangle. Additional details for computing these budgets over the ASTEX domain are contained in CSJ99.

Following Yanai et al. (1973), the apparent heat source Q_1 and the apparent moisture sink Q_2 can be interpreted as

$$Q_1 = Q_R + L(c - e) - \frac{\partial(\rho\overline{w's'})}{\rho\partial z}, \quad (3)$$

$$Q_2 = L(c - e) + L\frac{\partial(\rho\overline{w'q'})}{\rho\partial z}, \quad (4)$$

where Q_R is the radiative heating rate, c the rate of condensation, e the rate of evaporation of cloud water and rainwater, $s = c_pT + gz$ the dry static energy, and the primes denote deviations from the areal averages. The terms $\rho\overline{w's'}$ and $\rho\overline{w'q'}$ are vertical eddy fluxes of sensible and latent heat due to dry and moist turbulent and convective motions in the subcloud and cloud layers.

Subtracting (4) from (3), we obtain

$$Q_1 - Q_2 - Q_R = -\frac{\partial(\rho\overline{w'h'})}{\rho\partial z}, \quad (5)$$

where $h = c_pT + gz + Lq$ is the moist static energy and $\rho\overline{w'h'}$ is the vertical eddy flux of moist static energy. Assuming $\rho\overline{w'h'}$ is known at the surface $z = 0$ (e.g., from buoy data), integration of (5) yields

$$\rho\overline{w'h'}(z) = \rho_0\overline{w'h'}_0 - \int_0^z [Q_1(z') - Q_2(z') - Q_R(z')]\rho(z')\,dz'. \quad (6)$$

We note that $\rho_0\overline{w'h'}_0 = S_0 + \mathrm{LE}_0$, where S_0 and LE_0 are the supply of sensible and latent heat from the ocean surface, respectively, and the subscript "$_0$" denotes a surface value.

Cloud properties for this study were inferred using a

variety of observational platforms. Satellite-based estimates of low cloud amount were obtained from a special cloud classification dataset created for ASTEX by the French Meteorological Office/Centre de Meteorologie (CMS). This dataset, which is based on Meteosat data and processing techniques described in Séze and Desbois (1987), provides hourly estimates of various cloud types at a spatial resolution of 0.08°. Additional details of this dataset are given in CSJ99. Cloud top was deduced from sonde data by determining the inversion base (I_b).[1] Cloud-base measurements were available from 1-min ceilometer data at PS with a vertical resolution of 8 m. Ceilometer data from SM and VL were too irregular in time to provide a meaningful diurnal analyses of cloud base at these sites. Additional properties, such as column-integrated water vapor and cloud liquid water, were available at 1-min resolution from microwave radiometer retrievals taken at PS (Hogg et al. 1983). Also at PS the National Oceanic and Atmospheric Administration Environmental Technology Lab operated a K_α band cloud radar that produced very detailed images of cloud location and structure at 5 s and 37.5-m resolution (Martner and Kropfli 1993).

As part of the subduction experiment, surface measurements were available at a buoy located near the center of the ASTEX triangle (33°N, 22°W) as shown in Fig. 1. Using a vector averaging wind recorder (Weller et al. 1990), the buoy instrument system measured air and SSTs, barometric pressure, wind speed and direction, humidity, and radiative fluxes. The height of the meteorological observations taken on the buoy ranged between 2.4 and 3.5 m above sea level. Hourly values of these fields, as well as latent and sensible fluxes, computed using the bulk flux algorithm developed by Fairall et al. (1996), were obtained from the Woods Hole Oceanographic Institution. An overview of the subduction experiment datasets and results is given in Moyer and Weller (1997).

To obtain the diurnal variation of a given field, the data were subjected to a Kaiser window filter (Hamming 1989). For the 3-h sonde data an 11-point symmetric bandpass filter was employed. Data fields with a time resolution of less than an hour, were first averaged into hourly values. The hourly data were then subjected to a 23-point symmetric bandpass filter. The amplitude responses for these filters (shown in Fig. 2) are near 1.0 at 24 h and greater than 0.5 between 12 and 36 h. Because filtering requires an uninterrupted time series, data gaps are filled in by linear interpolation in time. When these gaps extended beyond a single period (e.g., due to missed sonde launches such as at VL during 4–6 June), the filtered data from these gap periods are not used. In effect, this filtering procedure isolates the diurnal signal from variability on other timescales, such as synoptic-scale frequencies. After filtering, the data are averaged by the time of day and the mean of the time series subtracted to obtain the hourly deviations.

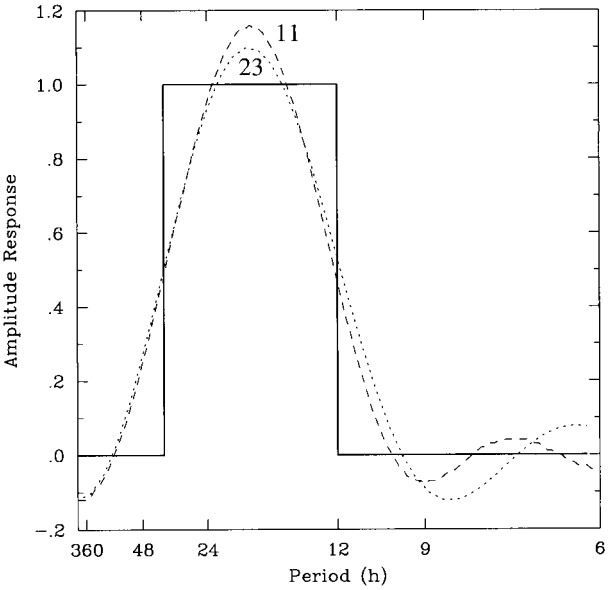

FIG. 2. Transfer functions for 11-point (dashed) and 23-point (dotted) symmetric bandpass filters described in the text. These filters were designed to isolate the diurnal frequency in the data by approximating the idealized filter shown here with a solid curve.

3. Diurnal variations over ASTEX

In this section we examine the diurnal variations of subcloud and cloud-layer properties over the ASTEX domain to gain some insight into the mechanisms that control the behavior of the diurnal cycle. These analyses use data from the 2-week period (1000 LST 1 June–0700 LST 15 June) when the ASTEX triangle of sounding sites was intact. We begin by presenting the diurnal cycle of surface fields from buoy observations, including the fluxes of sensible and latent heat. Next, we consider the daily variability of low cloudiness, including fractional coverage and vertical extent. Finally, using time–height diagrams, we examine the diurnal cycle of various parameters that enter into the heat and moisture budgets (temperature, water vapor mixing ratio, vertical motion), the budgets themselves, radiative heating, and the vertical eddy flux of moist static energy. In these time–height plots (based on 3-h sounding observations) the data is filtered, as described above, and the diurnal variability is expressed as deviations from the mean at each level.

A statistical summary of the fields considered in this paper is presented in Table 1. For each field the table lists the temporal mean, standard deviation (SD), diurnal amplitude[2] (DA), and the ratio DA/SD, which is a mea-

[1] The inversion base was determined with an automated procedure that searched each sounding starting at the 300-m level for a temperature inversion that was at least 100 m deep.

[2] The diurnal amplitude is half the diurnal range.

sure of the significance of the diurnal signal relative to the total field variance. In addition, spectral analyses were performed on time series of the fields listed in this table to determine the significance of the diurnal signal relative to a hypothetical red-noise spectrum. For this purpose, a chi-squared significance test was used with a hypothetical spectrum that was computed using the variance and lag-one autocorrelation of the time series as in Reynolds (1978). In general, the significance of the diurnal signal increases as the DA/SD ratio increases with ratios over 30% being significant at the 95% confidence interval, and ratios less than 10% having little, if any, significance in the diurnal frequency range.

a. Diurnal cycle of surface fields from buoy measurements

To examine the daily fluctuations of surface fields over the open ocean in ASTEX, we show in Fig. 3 the diurnal cycle of variables computed from measurements obtained from the buoy located near the center of the ASTEX triangle (see Fig. 1). The surface air temperature (T_0) peaks near local noon with a diurnal amplitude of approximately 0.23°C, while the SST exhibits a smaller diurnal amplitude (around 0.15°C) and lags T_0 by 3 to 4 h. A similar diurnal cycle in SST was observed in BOMEX. For example, the diurnal amplitude in the SST averaged from five BOMEX ships and over a 12-day period in June and July 1969 was 0.12°C (Delnore 1972). Since the saturation mixing ratio at the ocean surface (q*) shown in Fig. 3b is a function of SST, its diurnal variation follows that of the SST curve with peak values near 1430 LST and a diurnal amplitude near 0.13 g kg^{-1}. While the buoy-measured mixing ratio (q_ϕ), meridional wind component (v_0), and wind speed ($|v_0|$) show little or no significance in the diurnal frequency range (see Table 1), the zonal wind component (u_0) exhibits a modest diurnal variation from -1.2 m s^{-1} at 0300 LST to -1.7 m s^{-1} near local noon (Fig. 3c). The diurnal amplitudes in the ASTEX surface fluxes (Fig. 3d) are 3.6 W m^{-2} and 0.9 W m^{-2} for LE_0 and S_0, respectively, which are roughly 5%–10% of their daily mean values. While the mean $S_0 + LE_0$ in BOMEX ($\sim$200 W m^{-2}) is about double the ASTEX mean (CSJ99), it is unclear whether the diurnal amplitude of surface fluxes is also larger in BOMEX (Paulson et al. 1972; Holland 1972).

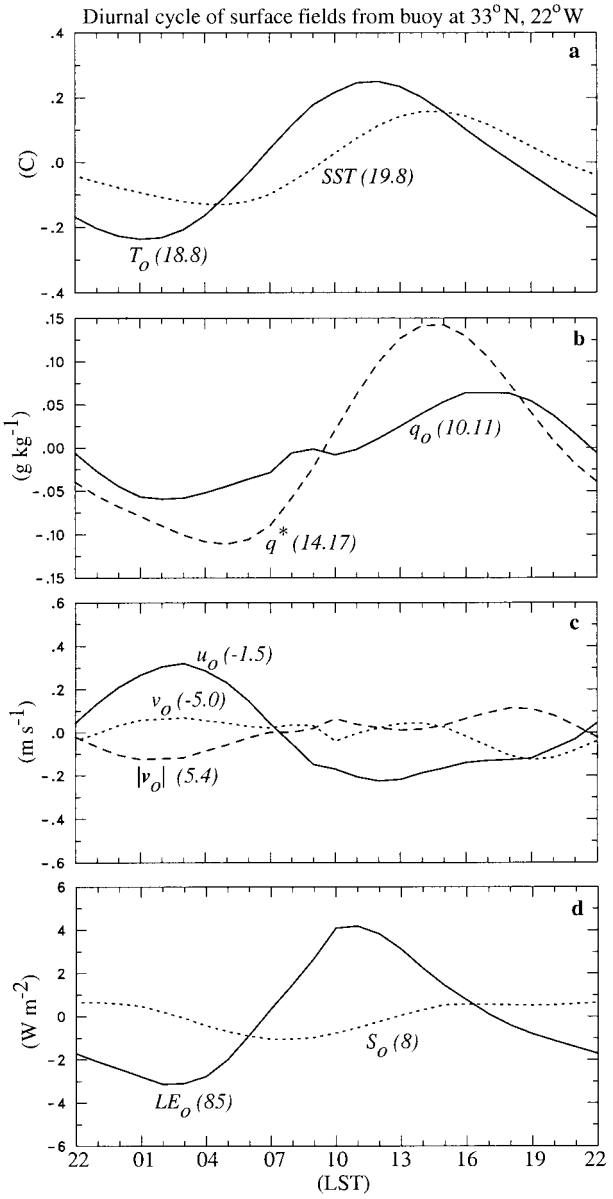

FIG. 3. Diurnal cycle of various surface fields computed from hourly buoy data for 1–15 Jun 1992. Buoy was located at 33°N, 22°W (near the center of the ASTEX triangle). (a) Variation of air (T_0) and sea surface temperature (SST), (b) variation of surface mixing ratio (q_0) and saturation mixing ratio at the ocean surface (q*), (c) variation of meridional (v_0) and zonal (u_0) wind components and wind speed ($|\mathbf{v}_0|$), and (d) variation of surface fluxes of sensible (S_0) and latent heat (LE_0). Numbers in parentheses next to curve identifiers represent the means for this 2-week period.

b. Diurnal cycle of low cloudiness

As deduced from the hourly CMS cloud classification analyses for 1–15 June 1992, the diurnal amplitude of fractional low cloudiness, σ, over the ASTEX triangle (Fig. 4a) is 7.2% with maximum coverage at 0500 LST and minimum coverage at 1430 LST. These characteristics of the diurnal cycle of low cloudiness are consistent with those deduced from International Satellite Cloud Climatology Project (ISCCP) satellite analyses over this region (Rozendaal et al. 1995). In Fig. 4b we show the diurnal variation of low cloud amounts for 1–15 June for circular areas with a 1° radius centered at the vertices of the ASTEX triangle. The average low cloud amounts for areas centered at SM, PS, and VL for this period are 58%, 47%, and 44%, respectively. This compares to ceilometer-based estimates of 68% at

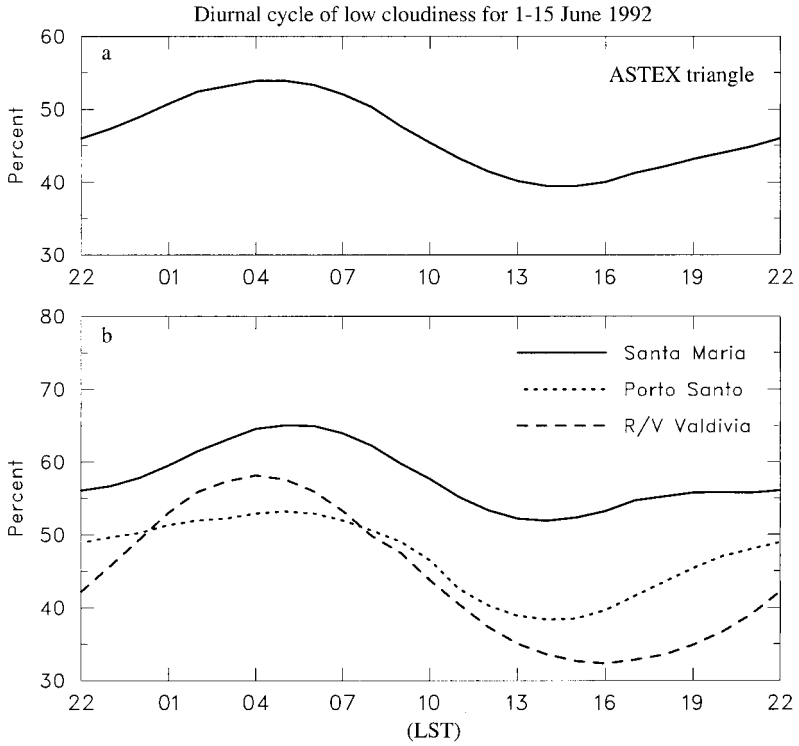

FIG. 4. Diurnal variation of fractional low cloudiness σ computed from hourly CMS analyses for 1–15 Jun 1992: (a) variation over the entire ASTEX triangle, and (b) variation over circular areas with a 1° radius centered at SM (solid), PS (dotted), and VL (dashed).

SM (for 4–23 June), 52% at PS (1–25 June), and 40% at VL (6–15 June) as reported by (Bretherton et al. 1995). The discrepancies between the satellite-based estimates and those from the ceilometers are most likely due to different averaging periods and to the presence of higher clouds that occurred about 7% of the time over the ASTEX region, obscuring the satellite's view of the lower clouds. The diurnal amplitude in low cloud amount as seen in Fig. 4b is 6.5% at SM, 7.5% at PS, and 13% at VL. This pattern of increasing diurnal range of low cloudiness at sites that are progressively equatorward and downwind in the mean flow is consistent with the findings of Rozendaal et al. (1995). They attribute this behavior primarily to solar radiative absorption within the clouds, which more effectively breaks up low clouds in deeper boundary layers.

Two distinctive features of the marine boundary layer thermodynamic structure over ASTEX are the trade inversion, typically 2–4 K in strength, and the transition layer, which marks the top of the well-mixed subcloud layer. These same features were also noted by Brill and Albrecht (1982) as being prominent characteristics of the trade wind boundary layer (as in ATEX and BOMEX). Comparison of these features in the PS sonde data to cloud radar and ceilometer observations show that the levels of the trade inversion and the transition layer are reasonable measures of cloud-top height (z_{ct}) and cloud-base height (z_{cb}), respectively (Stevens 1994). During ASTEX both the cloud top and base exhibited large variability on the synoptic timescale. For example, during 1–15 June the ASTEX-mean boundary layer cloud top varied[3] between 1200 and 1800 m, with fluctuations, related principally to changes in the large-scale subsidence rate, frequently exceeding 300 m (CSJ99). While no clear diurnal signal was present in z_{ct} at SM and VL (see Table 1)[4] and an incomplete record of ceilometer data made it difficult to analyze z_{cb} at these sites, a significant diurnal signal in the cloud boundaries was observed at PS. Because of this, and the fortuitous collocation of several instrument platforms at PS that can detect clouds and their properties (rawinsonde system, 8.7-mm Doppler cloud radar, laser ceilometer, and microwave radiometer), we will focus our discussion of the diurnal cycle of z_{ct} and z_{cb} at the PS site.

At PS the diurnal variation of cloud-top height (z_{ct}) is shown in the top panel of Fig. 5 for the 1–15 June 1992 period. Cloud-top height, inferred from the inversion base level in the sonde data, has a maximum (minimum) height at 2200 LST (1300 LST) with a daily amplitude around 90 m. Cloud radar analysis from PS

[3] The mean cloud top over ASTEX, as inferred from the inversion base level for this period, was 1460 m (CSJ99).

[4] In addition to the small DA/SD ratios for z_{ct} at SM and VL, their frequency spectra showed no significance relative to a red-noise spectrum in the diurnal frequency range.

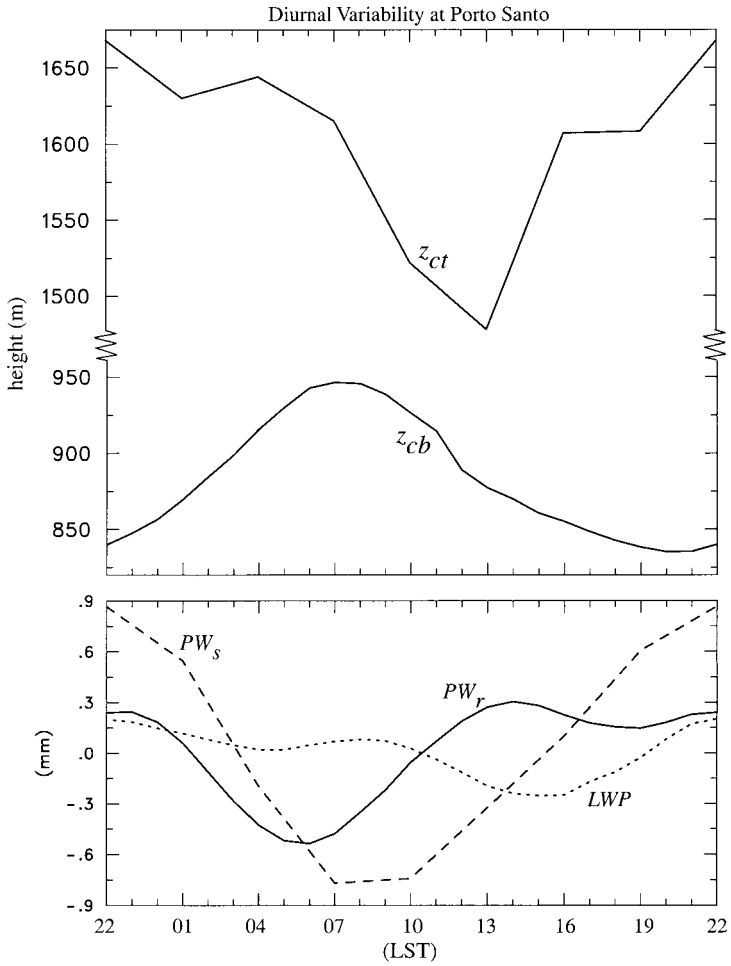

FIG. 5. Diurnal cycle of various cloud parameters at Porto Santo. Top panel: daily variation of cloud-top height (z_{ct}) inferred from sonde data and cloud base (z_{cb}) determined from ceilometer data. Bottom panel: daily variation of precipitable water (PW) at PS computed using sonde data (PW_s—dashed curve) and from radiometer measurements (PW_r—solid curve). Also from radiometer measurements at PS, the liquid water path (LWP) variation is shown by the dotted curve.

(not shown) of the cloud-top variation exhibits a similar phase behavior with a diurnal amplitude around 80 m. To understand the diurnal behavior of z_{ct} at PS, we consider the predictive equation for cloud-top height from a simplified cloud-topped mixed layer model (e.g., Lilly 1968). In this model, application of the budget equation for h to an infinitesimally thin layer at cloud top yields

$$\frac{\partial z_{ct}}{\partial t} = \overline{w}(z_{ct}) - \frac{\overline{(w'h')}_{ct} + \Delta F_R}{\Delta h}, \qquad (7)$$

where $\overline{w}(z_{ct})$ is the large-scale vertical velocity at cloud top, $\overline{(w'h')}_{ct}$ is the cloud-top moist static energy flux, and ΔF_R and Δh (which was typically negative in ASTEX) are the jumps in the radiative flux and h across cloud top, respectively. For simplicity in deriving (7) we have also assumed that there is no horizontal variation of z_{ct}. According to (7), cloud-top height changes over the ASTEX region are due to an imbalance between large-scale subsidence, which tends to shallow the mixed layer, and convective–radiative effects, which tend to deepen it. Because our line-integral techniques and budget analyses yield only the ASTEX area average of the terms on the right-hand side of (7), one can only speculate about the reasons for the diurnal behavior of z_{ct} at PS in Fig. 5. Later in this section we will present evidence that suggests that the diurnal variation of cloud top at PS is primarily controlled by convective–radiative effects.

The diurnal variation of cloud base (z_{cb}) at PS is also shown in the top panel of Fig. 5. The cloud base, as determined by ceilometer observations, averages 884 m with a diurnal amplitude of 56 m and a maximum (minimum) height near 0730 LST (2030 LST). The predawn rise in cloud-base height of 100 m is also seen in the diurnal ceilometer analysis of cloud base at VL and PS by White et al. (1995). The z_{cb} phase behavior in ASTEX

is somewhat different from that observed during the First ISCCP Regional Experiment (FIRE) in the stratus regime off the California coast (Betts 1990; Duynkerke and Hignett 1993) and in the trade wind regime of ATEX (Brill and Albrecht 1982), which showed an afternoon maximum in z_{cb}. As discussed later in this section, the diurnal behavior of z_{cb} in ASTEX appears to be related to the diurnal cycle of convective eddy activity.

The phase difference between the z_{ct} and z_{cb} curves at PS gives a maximum cloud thickness of 830 m at 2200 LST and a minimum of 600 m from 1000 to 1300 LST. This pattern of thinning clouds from night to day was also shown by Brill and Albrecht (1982) in ATEX for an undisturbed period in the trades and by Betts (1990) for California coastal stratus. However, in contrast to the results at PS, Betts' analysis shows little diurnal change in cloud top (similar to the z_{ct} behavior at SM and VL; see Table 1) and a rise in cloud base during the day. He attributes this behavior to solar heating of the cloud layer, resulting in daytime warming, stabilization of the subcloud layer, and decoupling of the cloud layer from the surface. The bottom panel of Fig. 5 shows the diurnal variation of liquid water path (LWP) at PS as measured by the microwave radiometer. Daily changes in LWP are related to variations in both cloud thickness and fractional coverage. In this regard, the daily maximum in LWP occurs at 2200 LST when fractional cloudiness at PS is around 50% (Fig. 4b), while the daily minimum occurs at 1400–1500 LST when cloudiness at PS is at a minimum around 38%.

Also shown in the bottom panel of Fig. 5 are the diurnal variation of column-integrated water vapor (i.e., precipitable water, PW) computed from PS sonde data (PW_s) and that measured independently by a microwave radiometer (PW_r). Hogg et al. (1983) demonstrated that the accuracy of PW measurements from a microwave radiometer is superior to that from conventional sonde data. Since approximately 70% of the PW (or 15 mm) is contained below the trade inversion, based on computations from PS sonde data, these curves essentially depict changes in boundary layer moisture. A comparison of these PW curves shows the diurnal amplitude of PW_s to be nearly double that of PW_r and while the radiometer shows that boundary layer moistening begins after sunrise (0600 LST), the moistening in the sonde data is delayed until after 1000 LST. We suggest that these differences underscore the difficulty that the PS sonde system had in accurately measuring diurnal changes in boundary layer moisture, that is, the tendency of the sonde humidity sensor at PS to produce excessive daytime drying in the boundary layer moisture field similar to that observed by Betts et al. (1995) in VL sonde data. Later in this section, an adjustment to the sonde moisture field, based on this PW comparison, is used to correct the Q_2 field and compute the vertical eddy flux of moist static energy.

c. Diurnal cycle of thermodynamic fields

The diurnal changes in the ASTEX-averaged potential temperature field (θ, top panel of Fig. 6) are strongly tied to the diurnal solar heating cycle, which peaks near 1200 LST during this period. There are two layers where the temperature fluctuations are most prominent: near the surface and in the inversion layer. The large temperature fluctuation near the surface results from the land sites (PS and SM), which have a diurnal temperature amplitude at the surface of 1.2°C, whereas buoy data (Fig. 3a) and VL sonde surface data give a more representative value for the open ocean over ASTEX of 0.25°C. The large diurnal temperature change in the inversion layer reflects variations of solar heating and cloud-top infrared radiative effects. The predawn minimum in this layer is likely due to diurnal fluctuations in fractional cloud coverage (Fig. 4), which peak around 0500 LST resulting in the greatest cooling at this time. The maximum warming near sunset in the inversion layer was also observed by Betts et al. (1995) in VL sonde data.

The variation in the ASTEX-averaged water vapor mixing ratio (q, bottom panel of Fig. 6) is marked by a late morning minimum and a nighttime maximum with the largest fluctuations confined to below the inversion level. Although the diurnal cycle of sonde surface q is inconsistent with that observed at the buoy (Fig. 3b), Table 1 indicates that the diurnal signal of q from the buoy has little or no significance. Within the boundary layer, moisture fluctuations are relatively constant with height with a diurnal amplitude about 0.32 g kg^{-1}. Similar diurnal amplitudes in boundary layer moisture were observed with sonde data in GATE (Albright et al. 1981) and in TOGA COARE (Johnson et al. 1996). Based on moisture analysis at VL from Betts et al. (1995) and at PS described earlier, we propose that the predawn (from 0000 and 0600 LST) drying tendency in Fig. 6 is real while the postdawn drying (from 0700 to 1000 LST) is due largely to sonde instrumental problems.

d. Diurnal cycle of kinematic fields

The diurnal cycles of vorticity (ζ) and divergence (δ) over ASTEX are shown in Fig. 7. Within the marine boundary layer the amplitude of the daily vorticity variation is about 1.4×10^{-6} s^{-1} or about 10% of its mean. This rotational field exhibits little phase change with height below 2 km, with a maximum anticyclonic flow around 0100 LST and a maximum cyclonic flow between 1000 and 1300 LST. The amplitude of the divergence diurnal cycle near inversion base is also about 1.2×10^{-6} s^{-1}, which is about 30% of its mean at this level (as reported in CSJ99). In contrast to the vorticity field, the divergence exhibits a more pronounced layered structure in the vertical with phase reversals about every 1 km. A maximum convergence (divergence) occurs at

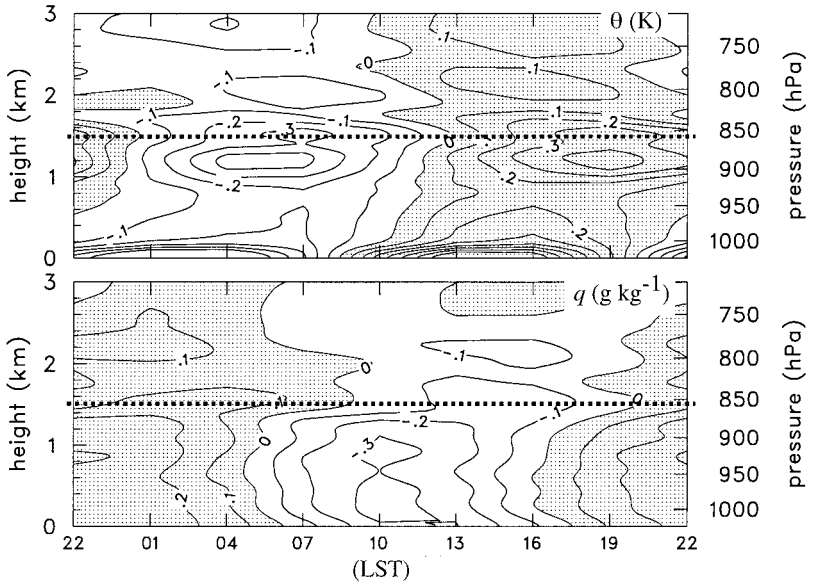

FIG. 6. Time–height sections showing the diurnal variation (as the deviation from the mean) over the ASTEX triangle of potential temperature θ (top panel, positive values shaded with increment 0.1 K), and water vapor mixing ratio q (bottom panel positive values shaded with increment 0.1 g kg^{-1}). Fields have been vertically smoothed with a 1-2-1 filter. Horizontal dotted line represents mean level of I_b over ASTEX for 1–15 Jun 1992.

the surface and near the I_b at 1000–1300 LST (2200 LST).

Figure 8 shows the diurnal cycle of winds for three 200-m-thick layers[5] centered around levels (600, 1500, and 2400 m) where the divergence field in Fig. 7 has amplitude maxima. This diagram was created by applying the diurnal filter to the winds at each level, then using all noninterpolated winds to create the layer average. At a given site and level, the winds generally show a regular clockwise turning in time with this pattern being most consistent during the daytime hours (0700–1600 LST) and less so at night. Focusing on the 1000 LST wind vectors (arrows with solid heads in Fig. 8) one can note at VL a clockwise turning of the winds with height (nearly 90°) between the lowest layers and a counterclockwise turning above. At SM a slight clockwise turning of the winds with height is observed between the lower two layers while at PS a slight counterclockwise turning with height occurs between the lowest layers and a large clockwise (nearly 180°) turning above. This diurnal wind shift between 1500 and 2400 m at PS largely accounts for the divergence sign change near 1.8 km in Fig. 7.

The divergence phase reversal near 1.8 km results in a vertical motion (w) maximum at this level with an amplitude of 0.12 cm s^{-1} (bottom panel in Fig. 7). This amplitude is about 20% of the mean subsidence rate of 0.6 cm s^{-1} at 1.8 km such that the ASTEX area-averaged subsidence rate varies diurnally from 0.48 cm s^{-1} at 1000 LST to 0.72 cm s^{-1} at 2200 LST. During the period of reduced subsidence drying (0700–1600 LST), which should be more conducive to cloud formation (other conditions being equal), Fig. 4 shows that the cloud fraction over ASTEX actually decreases. This suggests that factors other than large-scale subsidence (viz., radiative effects) are more important in determining the diurnal cycle of fractional cloudiness over ASTEX.

e. Diurnal cycle of heat and moisture budgets

The diurnal variations of Q_1 and Q_2 are presented in the time–height plots of Fig. 9. The basic structure of these fields is largely due to the local changes in θ and q (i.e., $\partial\theta/\partial t$ and $\partial q/\partial t$). This can be seen by noting how well the time changes of θ and q in Fig. 6 correlate with the maxima and minima in the Q_1 and Q_2 fields. While relatively small on synoptic and longer timescales, these local derivative terms dominate over the other terms in the budget equations (1) and (2) on a diurnal timescale. Closely linked to the diurnal solar heating cycle and consistent with the θ variations in Fig. 6, the Q_1 field exhibits daytime warming and nighttime cooling with the largest amplitudes in the lowest 100 m (due primarily to surface temperature changes at the land sites) and near the I_b level (due to cloud-top radiative effects). The Q_2 field shows a drying tendency that is strongest below I_b, begins near local midnight, peaks near sunrise, and extends into the late morning. The moistening tendency peaks in the late afternoon just below I_b. How-

[5] The effective resolution of the low-level ASTEX winds is about 200 m (Schubert et al. 1992).

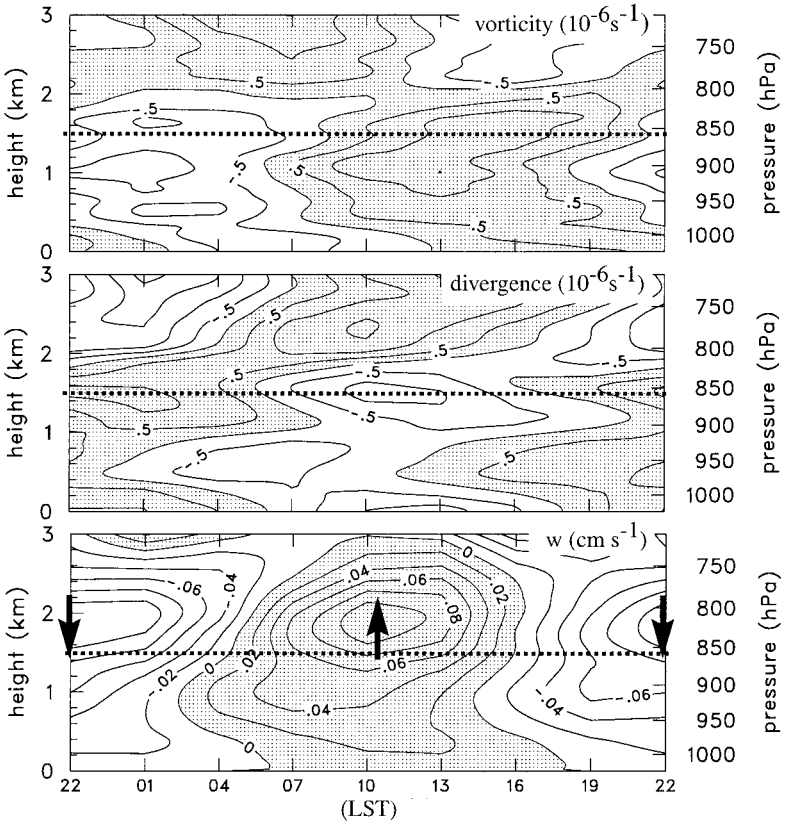

FIG. 7. Time–height sections showing the diurnal variation (as the deviation from the mean) of vorticity (positive values shaded with increment 0.5×10^{-6} s^{-1}), divergence (positive values shaded with increment 0.5×10^{-6} s^{-1}), and vertical motion with arrows indicating direction of flow (positive values shaded with increment 0.02 cm s^{-1}). The vorticity and divergence fields have been vertically smoothed with a 1-2-1 filter. Horizontal dotted line represents mean level of I_b over ASTEX for 1–15 Jun 1992.

ever, as noted from our earlier assessment of sonde humidity errors, these details of the diurnal Q_2 evolution should be regarded with caution.

f. Diurnal cycle of radiation and heat fluxes

Computation of the vertical eddy flux of moist static energy with (6) requires that the radiative heating be known. Since the goal here is to estimate the diurnal variation of radiative effects of clouds in the trade inversion layer over ASTEX, we simplify the problem by assuming a single cloud layer with constant bottom and top boundaries over the course of a day. Based on the average from the three ASTEX sounding sites, the cloud layer was centered at 1160 m with a thickness of 600 m, placing the cloud base and top at 860 and 1460 m, respectively. The liquid water mixing ratio, needed for radiative computations with clouds, was specified with the procedure described in CSJ99. Diurnal effects were included in this computation in the following ways, ordered here from least to most important in terms of their impact on the diurnal cycle of Q_R: thermodynamic structure of atmosphere, fractional cloudiness, and solar zenith angle. Although the profiles of q and T needed for the radiative computation are not adjusted to match the single cloud layer assumption, a sensitivity test where these fields were varied shows that this inconsistency has little effect on the Q_R results.

The procedure for computing $Q_R(z, t)$ involves the following steps. The National Center for Atmospheric Research community radiation model was run at 3-h intervals over the course of a day using diurnally varying atmospheric soundings to compute the radiative heating for clear Q_R^{clear} and cloudy Q_R^{cloudy} conditions. The clear-sky cases use ASTEX-averaged sonde temperature and moisture data, whereas the cloudy cases use the same thermodynamic data but augmented with the cloud information mentioned above. To choose a reasonable solar zenith angle for this computation, the radiation model was run for 7 June (i.e., the middle date of the 2-week period being examined) at the buoy position (i.e., a location at the center of the ASTEX triangle). To include the effects of the diurnally varying fractional cloudiness, the clear and cloudy profiles are weighted by σ (shown in Fig. 4a) to yield

$$Q_R(z, t) = \sigma(t)Q_R^{\text{cloudy}}(z, t) + [1 - \sigma(t)]Q_R^{\text{clear}}(z, t). \quad (8)$$

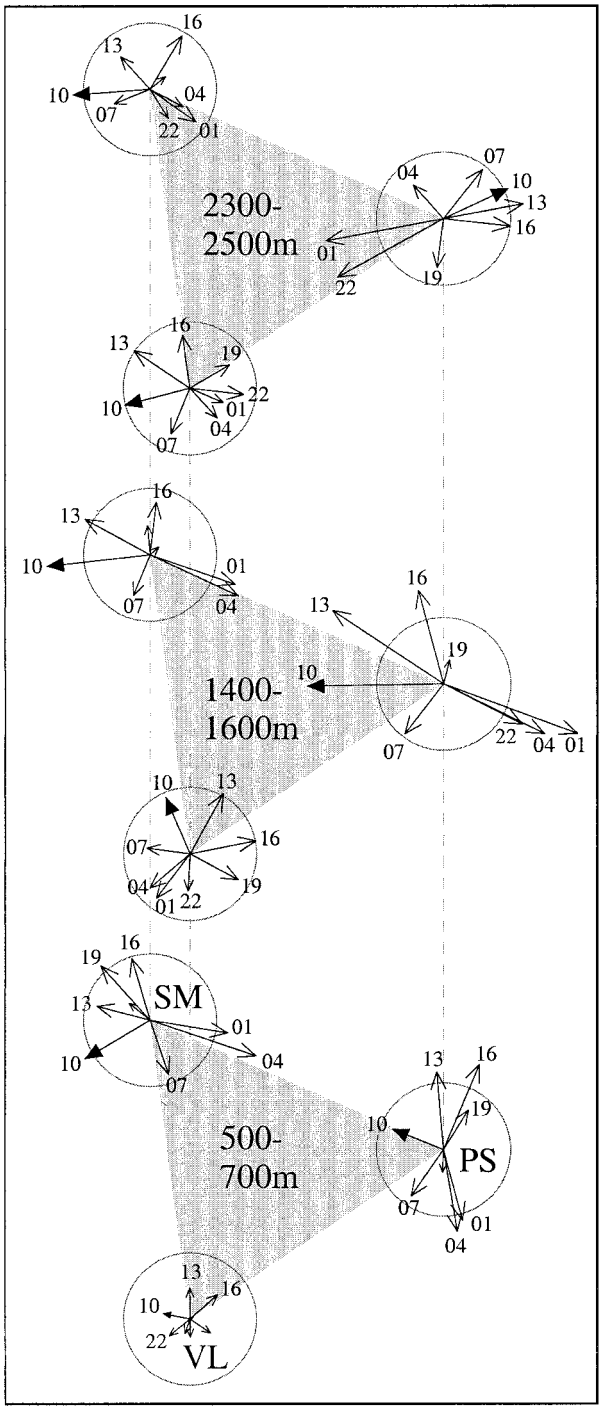

FIG. 8. Diurnal cycle of layer-averaged winds at three ASTEX sounding sites during 1–15 Jun 1992. Levels for layer averaging are indicated inside triangles. Circles centered at sounding sites have a radius of 0.5 m s^{-1}. Numeric labels near arrow heads indicate LST of wind vector. Wind vectors with magnitudes less than 0.2 m s^{-1} are not labeled.

Finally, the mean at each level is subtracted to produce the deviation diurnal heating field shown in Fig. 10a.

There are several features in the radiative field in Fig. 10 worth noting. First, this figure shows a diurnal amplitude in the vertically smoothed Q_R of 12.2 K day^{-1} near cloud top. In the nonsmoothed Q_R field (not shown) the diurnal amplitude is 38 K day^{-1} in a 25-m layer at cloud top. This compares to a diurnal amplitude of ~27 K day^{-1}, which we inferred from aircraft observations and theoretical flux profiles of marine stratocumulus taken near 60°N (Slingo et al. 1982). Normalizing these rates by the cosine of the zenith angles at local noon (9.3° for ASTEX and 43.7° for Slingo's estimates) brings them into closer agreement. Figure 10 also shows a peak cooling between 0400 and 0700 LST when fractional cloudiness is a maximum, and a cooling minimum (or deviation heating peak) at 1300 LST. The solar heating during the daylight hours extends deeper into the cloud layer than the nighttime longwave radiative cooling, which is confined to a shallow layer near the cloud top. This separation between the longwave cooling and shortwave heating peaks has some important implications. First, it tends to destabilize the cloud layer, which leads to a well-mixed cloud layer. Second, as the cloud layer warms due to solar radiative absorption, the upper part of the subcloud layer becomes stably stratified, which can lead to decoupling between the two layers. The nature of this decoupling on a diurnal timescale has been described in several previous investigations of stratocumulus regimes (e.g., Nicholls 1984; Duynkerke 1989; Hignett 1991; Miller and Albrecht 1995). As discussed in these studies, this decoupling process can lead to a thinning or even breakup of the cloud layer as solar absorption and dry air entrainment from above will cause evaporation of the cloud water, while the moisture supply at cloud base is reduced.

Diurnal variations of $\rho\overline{w'h'}(z)$ are highly sensitive to the sonde humidity errors alluded to earlier. For example, computation of $\rho\overline{w'h'}(z)$ using the diurnal variation of Q_2 shown in Fig. 9, with its inherent humidity problems, results in unrealistic fluxes particularly above I_b. To circumvent the sonde humidity errors in computing a diurnal heat flux field, an idealized humidity field is constructed and used to correct the local derivative term ($\partial q/\partial t$) in (2), that is, the major contributor to the Q_2 field on a diurnal timescale.[6] This idealized humidity field has the basic structure observed in the sonde humidity presented in Fig. 6 in that the amplitude of the diurnal $q(t)$ deviation is constant with height below I_b and then tapers to zero 200 m above I_b. Below I_b, the diurnal phase and amplitude of the idealized humidity field is constrained to match that observed by the radiometer at PS; that is, the PW_r curve in Fig. 5,

[6] Correcting the horizontal and vertical advection terms in (2) for sonde errors would have added a level of complexity that is unwarranted by the small magnitude of these terms in comparison to the local derivative term on a diurnal timescale.

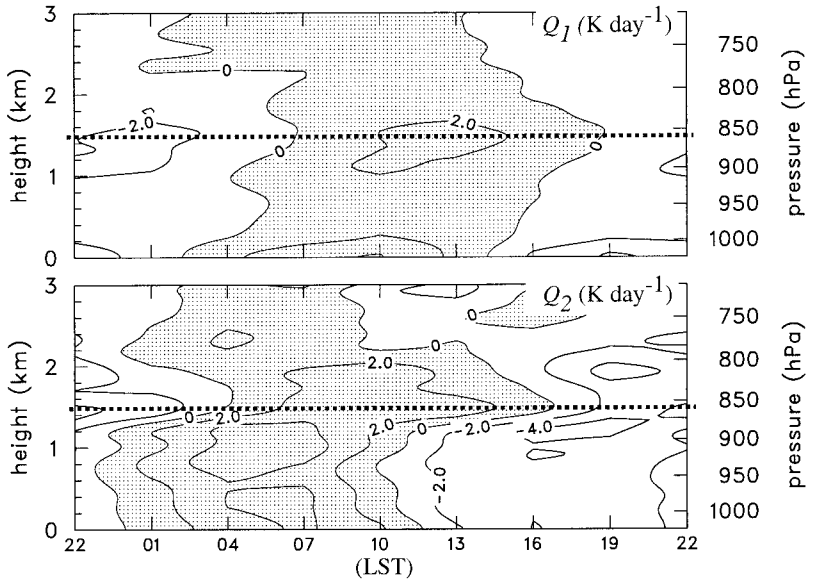

FIG. 9. Time–height sections showing the diurnal variation (as the deviation from the mean) over the ASTEX triangle of apparent heat source Q_1 and apparent moisture sink Q_2 (positive values shaded with increment 2 K day^{-1}). Fields have been vertically smoothed with a 1-2-1 filter. Horizontal dotted line represents mean level of I_b over ASTEX for 1–15 Jun 1992.

which appears to more accurately capture diurnal boundary layer moisture changes than sonde data.

Using this idealized diurnal humidity field to compute the local derivative term ($\partial q/\partial t$) in (2), results in the ''corrected'' Q_2 field shown in Fig. 10b. In this figure the drying rates below I_b more closely match the humidity tendencies observed from the PS radiometer than those presented in Fig. 9. Specifically, the drying rates in Fig. 10 are about two-thirds their magnitude in the ''uncorrected'' Q_2 field (Fig. 9), and the time of peak drying, which occurs at 0400 LST in Fig. 10 more closely matches the radiometer observations in Fig. 5. In addition, the period of strong moistening around 1300 LST in the ''corrected'' Q_2 field correlates well with the decrease in liquid water at this time as denoted in the LWP curve from PS in Fig. 5.

The diurnal cycle of the vertical eddy flux of moist static energy is computed from (6) using the diurnal fields of Q_1 in Fig. 9, and the Q_R and corrected Q_2 in Fig. 10. The integration of (6) begins at $z = 0$ where the diurnal variation of the surface flux term, $\rho_0 \overline{w'h'}_0$, is given by the sum of the sensible and latent heat flux curves shown in Fig. 3d. Evaluation of (6) using this procedure yields the $\rho \overline{w'h'}$ field shown in the bottom panel of Fig. 10. The diurnal cycle of this eddy flux field shows a peak amplitude near 1.2 km with a daily amplitude near this level of 38 W m^{-2}. The maximum fluxes at 0400 LST and minimum fluxes near local noon (1000–1300 LST) correspond well with the nighttime enhancement and daytime thinning of the low-cloud layer (Fig. 4). The range of fluxes is shown more clearly in Fig. 11 where the daily mean flux profile (presented in CSJ99 Fig. 8) has been added to the diurnal signals at these times. These results are qualitatively consistent with computations from a simple mixed layer model presented in Schubert (1976). In simulating the diurnal cycle of the stratocumulus regime off the California coast, Schubert showed that the turbulent flux just below the cloud top peaked during the nighttime hours at ~60 W m^{-2} and was a minimum near local noon around 20 W m^{-2}. A similar enhancement in the nighttime turbulence was shown by Duynkerke and Hignett (1993) in the marine boundary layer during FIRE with observations and model simulations. In their daytime analyses, two distinct peaks were observed in the vertical profile of turbulent kinetic energy, one near the surface and a second smaller peak in the cloud layer. In our analysis (Fig. 11), there is only a slight indication of a secondary maximum near the cloud top in the daytime flux profile.

Thus far, the diurnal analyses of radiation and moist static energy have been presented for an idealized cloud layer with a 600-m thickness. However, as alluded to earlier, cloud boundaries during ASTEX varied significantly on a synoptic timescale, as well as from site to site (note the large standard deviations in z_{ct} and z_{cb} in Table 1). For this reason, a sensitivity test was conducted to get a sense for how changes in cloud thickness affect these analyses. In this test, the cloud layer was centered at 1160 m and its thickness varied from 200 to 1000 m about this level. Results of this sensitivity test show that the primary effect of cloud thickness changes is on the daytime vertical heating structure. That is, as the cloud depth increases the separation distance between the

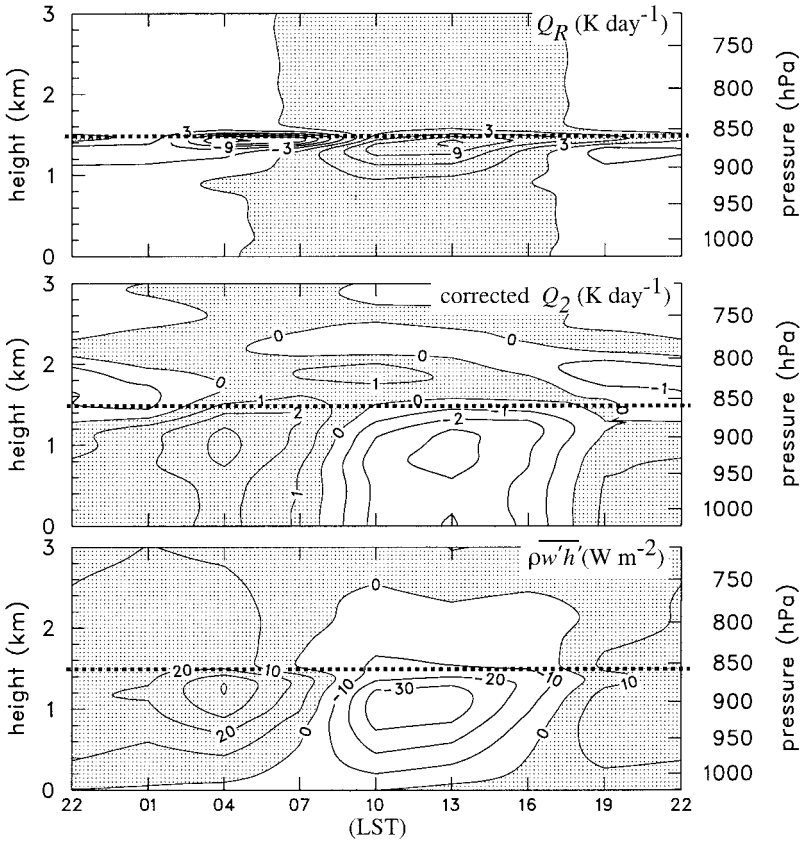

FIG. 10. Time–height sections showing the diurnal variation (as the deviation from the mean) of radiative heating Q_R (top panel, positive values shaded with increment 3 K day^{-1}), corrected Q_2 (middle panel, positive values shaded with increment 1 K day^{-1}), and the vertical eddy transport of moist static energy (bottom panel, positive values shaded with increment 10 W m^{-2}) based on data from 1 to 15 Jun 1992. Fields of Q_R and corrected Q_2 have been vertically smoothed with a 1-2-1 filter. Horizontal dotted line represents mean level of I_b over ASTEX for 1–15 Jun 1992.

peaks of longwave cooling at cloud top and shortwave heating within the cloud layer also increases (results not shown). In deeper cloud layers this increased separation distance results in weaker instability (and thus mixing) within the cloud layer. To summarize, this sensitivity test shows that while changes in cloud layer thickness have little impact upon radiation and the vertical eddy flux profiles at night and in the daytime subcloud layer, during the daytime hours radiative feedbacks in thicker cloud layers will result in weaker mixing profiles within the cloud.

In Fig. 10 we note that the eddy flux maximum at 0400 LST is contemporaneous with the drying peak in the corrected Q_2 field, with a similar correspondence between the flux minimum and the moistening peak near local noon. Using a one-dimensional time-dependent model to study diurnal variations in the trade wind boundary layer, Brill and Albrecht (1982) found a similar relationship between convective activity and drying/moistening tendencies in the subcloud layer. Their results showed that the early morning convection was relatively active, which results in a drying of the subcloud layer due to an enhanced moisture transport out of this layer by the convective elements. The enhanced moisture transport out of the subcloud layer would tend to humidify the cloud layer, other conditions being constant. However, during the predawn hours cloudiness increases, reaching a maximum around 0500 LST (Fig. 4). It would appear that condensation is converting the additional water vapor flux into the cloud layer to liquid (consistent with the cloudiness increase and observed drying tendency in the cloud layer at this time). Conversely, a late afternoon moistening of the subcloud and cloud layers occurs when convection is less active and clouds evaporate. Brill and Albrecht also note that the early morning drying of the subcloud layer results in a higher cloud base at this time. Consistent with this observation, the cloud base (z_{cb}) at PS is highest at 0700 LST (Fig. 5) just prior to the moistening trend in the subcloud layer depicted in the corrected Q_2 field in Fig. 10. We also note in Fig. 5 that the diurnal trend in cloud-top height (z_{ct}) at PS correlates well with observed trend

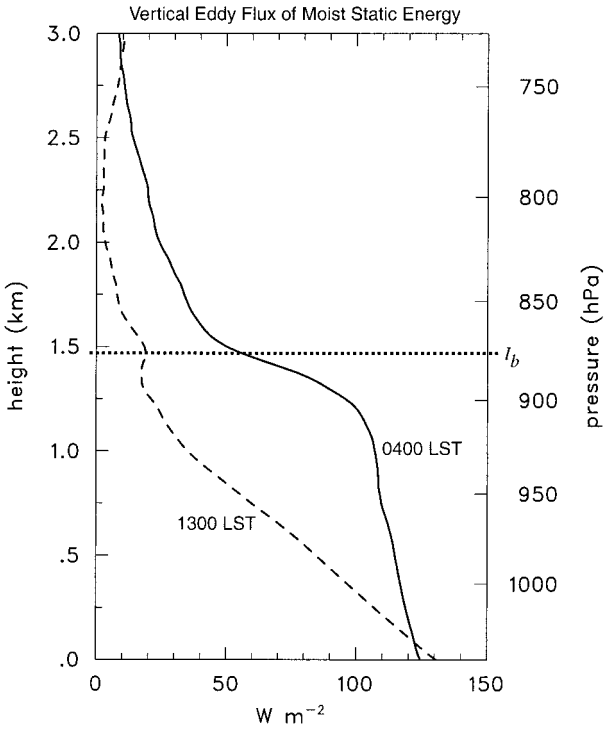

FIG. 11. Vertical profiles of the vertical eddy transport of moist static energy at 0400 LST (solid) and 1300 LST (dashed) for the ASTEX region. Horizontal dotted line represents mean level of inversion I_b over ASTEX for 1–15 Jun 1992.

in the vertical eddy flux field in Fig. 10 (i.e., decreasing z_{ct} at PS is concurrent with decreasing convective activity). If one considers the change in z_{ct} in (7) due only to the effect of large-scale subsidence [i.e., the first term on the right-hand side of (7)], then the observed diurnal amplitude in $\overline{w}(z_{ct})$ of 0.1 cm s^{-1} yields a cloud-top diurnal amplitude of ~14 m. Since this is much smaller than the 90-m diurnal amplitude observed at PS, it seems reasonable that the effects of convection/radiation [i.e., the second term on the right-hand side of (7)] as depicted in the bottom panel of Fig. 10 are largely responsible for the observed cloud-top behavior at this site. While reasons for the lack of a diurnal signal in z_{ct} at SM and VL (see Table 1) are uncertain, it seems likely that the cloud-top balance between the large-scale subsidence and convective–radiative effects at these sites was different from that which occurred at PS.

In this section we have shown the importance of cloud radiative processes in determining the diurnal characteristics in several fields including: boundary layer moisture and temperature, vertical eddy fluxes, fractional cloudiness, and cloud boundaries at PS. On a diurnal timescale, fluctuations in these fields correlate poorly with those in the kinematic fields (Fig. 7), which suggests that the large-scale forcing due to low-level divergence is of secondary importance over the ASTEX region as a whole. A similar conclusion, based on observations and model results, was reached by Brill and Albrecht (1982), who state that the diurnal variation of the trade wind boundary layer in ATEX is ''primarily due to the diurnal variation of radiative forcing and secondarily to diurnally varying large-scale divergence.''

4. Diurnal cycle over the North Atlantic

Thus far we have focused on the diurnal cycle for a 2-week late spring period over the ASTEX domain. To provide a larger-scale context for these results we now examine the diurnal variability of divergence and vertical motion in adjacent regions of the North Atlantic. These fields have been examined in some detail in previous studies because of their importance to convection and precipitation.

Figure 12 compares the divergence averaged in the lowest 1500 m for a 2-week period in ASTEX to that for a 6-day undisturbed period (7–12 February 1969) in the trade winds from ATEX (Brill and Albrecht 1982). While the time-mean low-level divergence is quite similar in these two regions, the diurnal amplitude for

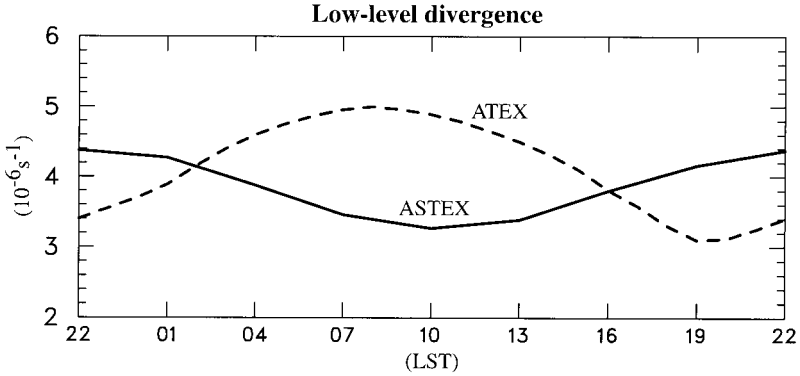

FIG. 12. Diurnal variation of the surface to 1500-m mean divergence (10^{-6} s^{-1}) during an undisturbed period for ATEX (dashed line) from Brill and Albrecht (1982) and from 1 to 15 Jun for ASTEX (solid line).

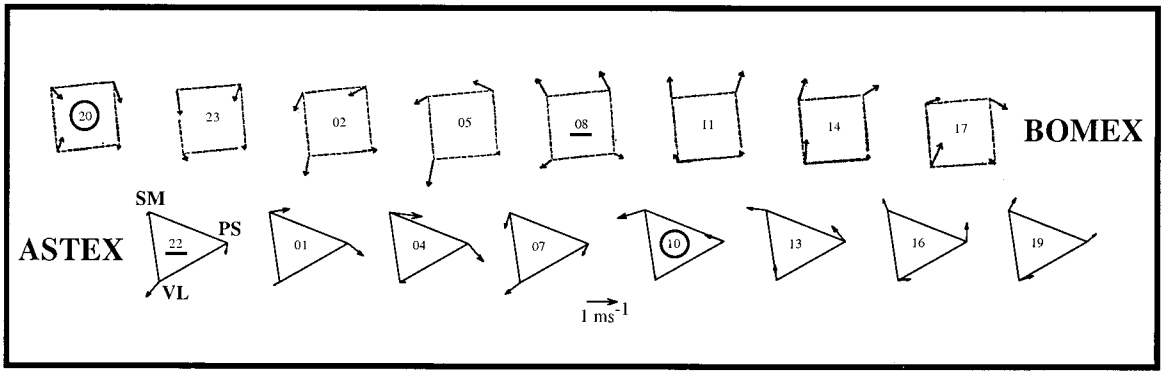

FIG. 13. Diurnal variation of wind vectors in (top row) BOMEX at $p^* = 90$ hPa (~1 km) and in (bottom row) ASTEX averaged from the surface to 1500 m. The numbers in the polygons indicate the local time of the observations. For each experiment the circled number indicates the time of maximum low-level convergence while the underlined number indicates the time of maximum low-level divergence. Rows are shifted slightly so that their time axes line up.

ATEX is significantly larger (1.0×10^{-6} s^{-1}) than that in ASTEX (0.6×10^{-6} s^{-1}).[7] In addition, the diurnal variation of low-level divergence is nearly 180° out of phase with a maximum in ATEX near 0800 LST as opposed to 2200 LST in ASTEX.

Yet another comparison to diurnal circulations in trade wind flow is provided by analyses from BOMEX. The diurnal amplitude of divergence in BOMEX (not shown) averaged in the lowest few kilometers is about 1.5×10^{-6} s^{-1} (Nitta and Esbensen 1974a), which is larger than in both ATEX and ASTEX. The diurnal variation of the low-level wind vectors in BOMEX for the period 22–30 June 1969 is compared to that from ASTEX (0–1500-m layer averaged winds) for the period 1–15 June 1992 in Fig. 13. From this diagram we note that the low-level divergent flow in BOMEX peaks near 0800 LST, consistent with that observed in ATEX, and nearly out of phase with the flow in ASTEX. At the northern ships of BOMEX and the sites of SM and PS in ASTEX the diurnal wind vectors show, for the most part, a regular anticyclonic turning during the course of a day. On the other hand, at the southern ships of BOMEX the wind vectors show a more complex diurnal pattern, which Nitta and Esbensen attribute to local effects. The complex diurnal pattern observed at VL in Fig. 13 results from averaging the winds over a layer characterized by significant phase change with height (Fig. 8). Finally, we note that the diurnal wind signal in both regions is such that winds blow away from the continent (see Fig. 1) during the day and toward it at night, which is in the opposite sense of a local land–sea-breeze circulation. Some possible explanations for this flow behavior will be considered shortly.

The stronger diurnal cycle in BOMEX and its out-of-phase relationship compared to ASTEX are also evident in the vertical mass flux (ω) comparison in Fig. 14. Here the diurnal amplitude of vertical mass flux in BOMEX is more than twice as large as that observed in ASTEX. (Note that the contour interval is greater in the BOMEX analysis.) With a mean subsidence rate near inversion base in BOMEX of 2.0 hPa h^{-1}, its vertical mass flux varies from 1 hPa h^{-1} at 2000 LST and 3 hPa h^{-1} at 0800 LST. In ASTEX a more modest diurnal modulation is observed with subsidence rates varying between 2.95 hPa h^{-1} at 2200 LST and 2.05 hPa h^{-1} at 1000 LST. It is also noteworthy that in both of these regions the peak diurnal amplitude of vertical mass flux occurs above and within 0.5 km of the inversion base. The proximity of these peaks to the cloud top may suggest that cloud-top radiative effects are playing a role in determining the diurnal characteristics of low-level divergence and vertical motion in these regions. McBride and Gray (1980) have suggested that the diurnal modulation of vertical motion over these oceanic regions is a dynamical response to the daily cycle of radiative cooling, which is enhanced by low-level cloudiness in the stratocumulus regimes.

Nitta and Esbensen (1974a) have suggested that diurnal variations of low-level flow in BOMEX shown in Figs. 13 and 14 are a remote response to land–sea heating contrasts from the South American coast. At first glance such an explanation seems implausible since the center of the BOMEX array was about 800 km from the South American coast and the diurnal cycle of its low-level winds were in the opposite sense from a typical land–sea breeze circulation (Fig. 13). However, in support of this mechanism, Sun and Orlanski (1981) found that an interaction between trapeze instability (Orlanski 1973) and a sea-breeze circulation resulted in a diurnal pattern of vertical motion a few hundred kilometers off the coast, consistent in many aspects to that observed in BOMEX (Fig. 14). Rotunno (1983) further elucidated Sun and Orlanski's results using linear theory to study land–sea breeze circulations. Rotunno found that the response to a diurnally varying land–sea heating contrast differs dramatically depending on the latitude

[7] This smaller diurnal amplitude for the 0–1500-m ASTEX mean divergence is due in part to its phase changes with height in this layer.

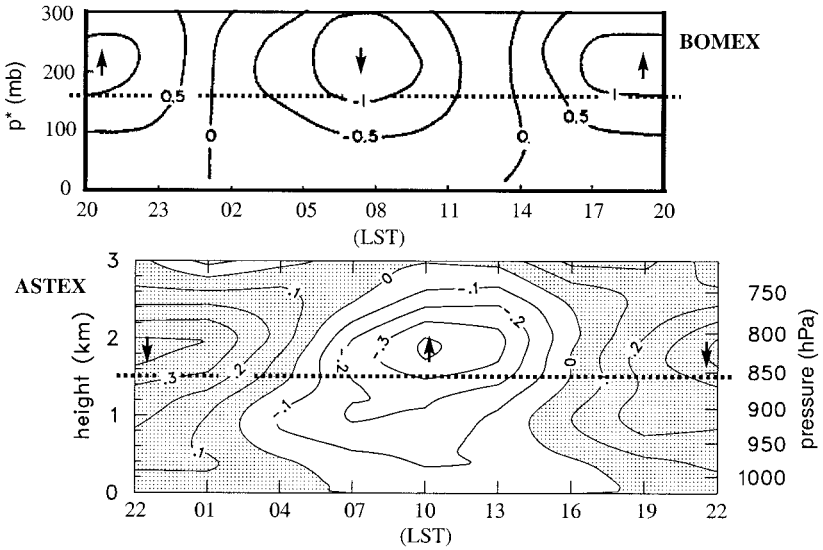

FIG. 14. Time–height sections showing the diurnal variation (as the deviation from the mean) of vertical motion (hPa h^{-1}) in (a) BOMEX (top panel, after Nitta and Esbensen 1974) and (b) ASTEX (bottom panel). Contour increment is 0.5 hPa h^{-1} in top panel and 0.1 hPa h^{-1} in bottom panel. Arrows indicate direction of motion. To facilitate this comparison the plots are shifted slightly so their time axes line up.

of the forcing. For latitudes equatorward of 30° he found the response to be in the form of internal-inertial waves with a resulting circulation, as in BOMEX, which is nearly out of phase with the heating.

Under favorable atmospheric conditions (warm season surface heating and light winds), Mahrer and Segal (1985) modeled a local sea-breeze circulation for elongated, small island (infinite length, 5-km half-width) with a diurnal amplitude of vertical motion around 10 cm s^{-1}. In contrast, weak surface heating (a diurnal amplitude around 1°C), and moderate low-level northeasterlies, inhibit any local sea-breeze circulations at the islands of PS and SM (which have elongated shapes with areas less than 50 km^2). However, could a sea-breeze circulation from the African continent influence the diurnal flow pattern observed over ASTEX[8] as shown in Figs. 8 and 13? As a related question, could the larger island of Madeira (with an area ~600 km^2) located about 60 km to the southwest of PS affect the flow characteristic at this site? To address these questions, the Regional Atmospheric Modeling System (RAMS) was used investigate the possible effects of the African and Madeira land–sea breezes on the flow over ASTEX (experiments performed courtesy of Roger Pielke Sr. and John Strack of Colorado State University). A description of the model configuration, experimental design, and details of the results are given in the appendix.

In brief, these RAMS simulations showed enhanced afternoon subsidence at PS. Not only is this inconsistent with the diurnal cycle of ASTEX-averaged vertical motion (Fig. 7), but such a pattern of vertical motion would likely result in descending cloud tops [from the cloud-top equation (7)] and rising cloud bases (as a result of entrainment of subsident air into the marine boundary layer causing a warmer, drier subcloud layer), which is just the opposite of cloud boundary trends observed at PS in Fig. 5. Finally, the mean low-level flow during ASTEX, out of the north-northeast at greater than 5 m s^{-1} (CSJ99), would mitigate any sea-breeze effects from Madeira at the upstream location of PS. From these preliminary simulations we conclude that the land–sea-breeze circulations from Africa and Madeira are having little, if any, effect upon the diurnal flow field observed at PS, and more generally over ASTEX.

Figure 15 (from Albright et al. 1981) shows the time–height section of vertical motion averaged over all three phases of the GATE B-scale network. In this diagram, constructed using 6-hourly sounding data, the time-mean vertical motion in each layer has not been removed. This analysis shows upward motion occurring at all times and all levels below 750 hPa. The peak upward motion with a rate of 4.7 hPa h^{-1} occurs at 1030 LST between 700 and 800 hPa. At 2230 LST subsidence occurs above 750 hPa with weak upward motion ($<$1.0 hPa h^{-1}) below this level. While the diurnal cycle of vertical motion has a much deeper and stronger signal in the convectively active GATE region, the phase is similar to that in observed in ASTEX with diurnal deviation low-level convergence observed in late morning. Several studies (e.g., Gray and Jacobson 1977; McBride and Gray 1980; Dewart 1978) have noted that the late

[8] The center of ASTEX triangle was located about 1100 km off the northwest coast of Africa with PS being the closest offshore site about 750 km from the coast.

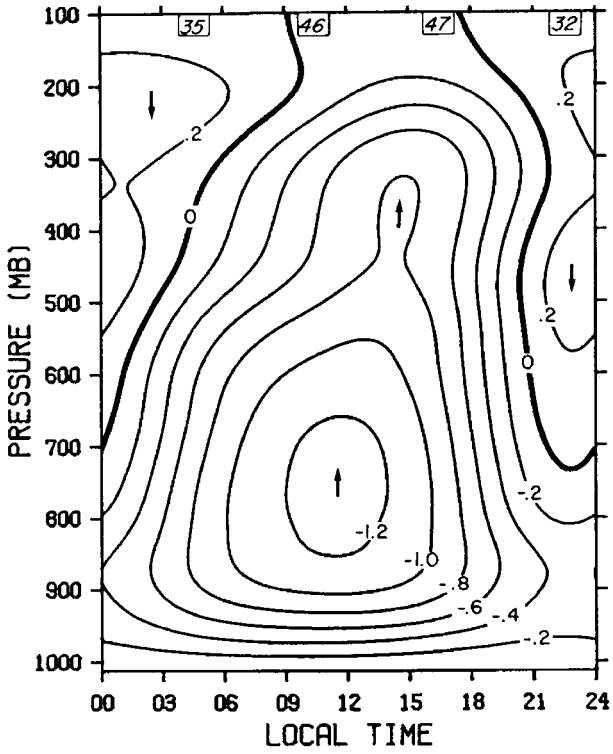

FIG. 15. Time–height section showing the diurnal variation of vertical motion (10^{-3} hPa s^{-1}) averaged over all three phases of GATE (after Albright et al. 1981). Numbers below the upper margin show the number of cases used in computing the hourly means. (Note: 1.0 $\times$ 10^{-3} hPa s^{-1} = 3.6 hPa h^{-1}.)

morning maximum in low-level convergence precedes the rainfall maximum in GATE by ~6 h. These studies have postulated that the delay in convection over GATE may be due to the large low-level vertical shear and lapse-rate stability over the GATE region, which acts to delay convective development by a few hours after the peak in low-level convergence.

Recently Dai and Deser (1999) have examined the diurnal cycle of surface winds and divergence over much of the globe. Figure 16 (with analysis provided by A. Dai) shows the phase of the summertime mean surface divergence over the North Atlantic. This analysis is based on 3-hourly wind observations from both land and marine reports from the period 1976–97. Dai and Deser note that their phase analysis may contain large uncertainties (±1.5 h) especially over oceanic regions where observations are more sparse. The corresponding diurnal amplitude diagram (Fig. 9 of Dai and Deser 1999) shows that the amplitude of summertime surface divergence varies from 2.0 $\times$ 10^{-7} s^{-1} over the midocean regions to 3.0–5.5 $\times$ 10^{-7} s^{-1} over the continents. These oceanic divergence amplitudes are somewhat less than the values reported in the budget experiments in this paper (0.6–1.5 $\times$ 10^{-6} s^{-1}), which likely results from more smoothing in time and space in the Dai and Deser analysis.

Superimposed on Fig. 16 are the sounding arrays, shown as polygons, from three field campaigns conducted during the summer months over the North Atlantic (ATEX being excluded here because it was held

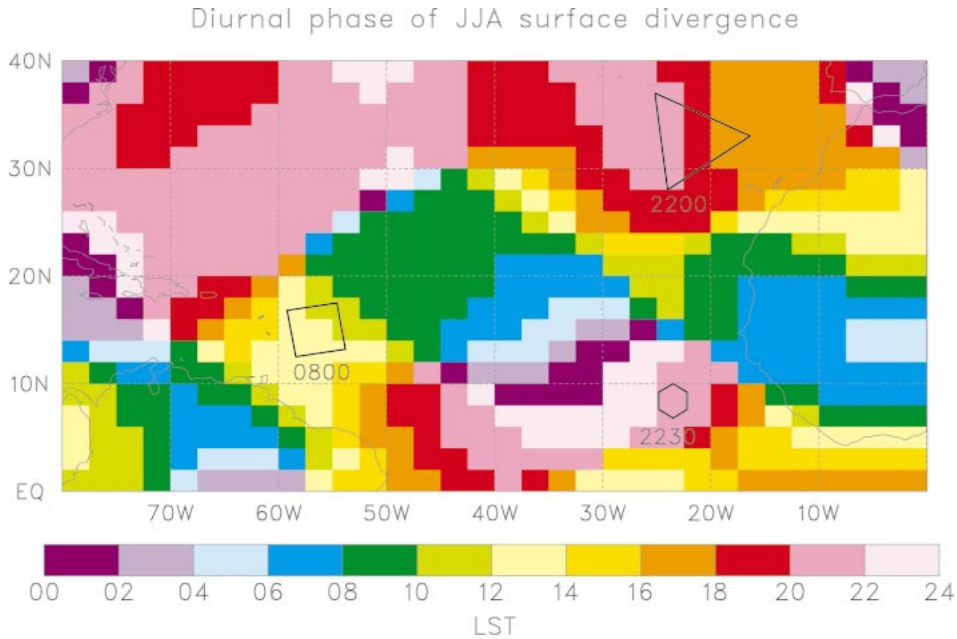

FIG. 16. Diurnal phase of surface divergence for the summer months of JJA (Jun–Aug). Phase data provided by A. Dai (2000, personal communication). Also shown are the polygons locating three summertime field experiments. The numbers listed below each polygon indicate the hour in LST at which surface divergence was observed to be a maximum in each of these experiments. The averaging period is 8 days for the BOMEX result, 14 days for the ASTEX result, and 59 days for the GATE result.

during the winter season). For comparison to Dai and Deser's analysis, listed next to each polygon is the local time at which surface and low-level divergence was observed to maximize in each of these experiments. Considering the different averaging periods for these estimates (listed in the figure caption), the overall comparison to Dai and Deser's analysis is quite favorable with the phases being within an hour for GATE, a few hours for ASTEX, and about 4 h for BOMEX. Over the ASTEX domain Dai and Deser's phase analysis varies from 1700 UTC near the eastern edge to 2100 UTC near the western edge. Such phase differences across the ASTEX domain suggest that our computations of area-averaged quantities (such as the diurnal amplitudes of divergence and vertical motion) have been smoothed and most likely are underestimated.

Another interesting feature in the phase analysis in Fig. 16 is the alternating phase in the latitude belts across the North Atlantic. For example, within the trade wind belt (14°–22°N) the phase peaks around 1100 LST, which is out of phase with the Atlantic ITCZ belt to its south (4°–12°N) with peak phase around 2300 LST and with the stratocumulus regime to its north (26°–40°N) with peak phase around 2000 LST. This pattern of alternating phase in the surface divergence is observed in both the Atlantic and Pacific Oceanic basins in the annual mean phase analyses (Dai and Deser 1999). The phase difference between the adjacent trade and the ITCZ regions in the North Atlantic is evidence for a diurnally pulsing Hadley cell. Dai and Deser note that this meridional circulation runs strongest during the late morning hours when convergence is a maximum in the ITCZ and divergence is a maximum in the trade wind belt. The diurnal modulation of the Hadley cell over the GATE region was discussed by McBride and Gray (1980), who postulated that enhanced nighttime radiative cooling in the stratocumulus regime to the north of the ITCZ results in a local increase in large-scale subsidence. With a response lag of several hours this enhanced subsidence will in turn cause an increase in the low-level convergence of mass into the ITCZ. While the phase differences depicted between the trades and ITCZ regions in Fig. 16 support McBride and Gray's general findings of a diurnally modulated Hadley cell, how the diurnal variability of mass flux within the stratocumulus regime fits into this picture is less clear.

5. Summary and concluding remarks

A variety of observations and model-generated radiative heating profiles have been used to examine the diurnal variability of various fields over the ASTEX domain. A summary of the major findings are listed here.

- On a diurnal timescale, low cloudiness over the ASTEX triangle varies from a maximum of 54% around 0500 LST to a minimum of 39% around 1500 LST (Fig. 4). While low cloudiness decreases from north to south across the ASTEX domain, its diurnal variation increases.
- A phase reversal in divergence near 1.8 km results in a diurnal vertical motion maximum near this level. At this level the ASTEX area-averaged subsidence exhibits a modest diurnal modulation varying from 2.05 hPa h^{-1} at 1000 LST to 2.95 hPa h^{-1} at 2200 LST. Recent global analysis of diurnal surface divergence reveals large regional variability over the North Atlantic. Since the ASTEX triangle covers such a large area, its analysis of low-level divergence and vertical motion will be influenced by this spatial variability.
- Model-generated radiative heating profiles (Fig. 10) show a maximum cooling near cloud top between 0400 and 0700 LST and a minimum in cooling (deviation heating) at 1300 LST, which extends deeper into the cloud layer. During the daytime hours, the longwave cooling near cloud top and shortwave heating within the cloud layer tend to destabilize the cloud layer, leading to a well-mixed cloud layer. Also, as the cloud layer warms it becomes stably stratified relative to the subcloud layer. This can lead to decoupling between the two layers. Consistent with the diurnal cycle of fractional cloudiness in Fig. 4, this decoupling leads to a thinning or even breakup of the cloud layer as solar absorption and dry air entrainment from above will cause evaporation of the cloud water, while the moisture supply at cloud base is reduced.
- Budget equations are used with a humidity-corrected Q_2 field and diurnally varying radiation profiles to compute the diurnal cycle of vertical eddy fluxes of moist static energy for ASTEX. The results show a diurnal amplitude in this eddy flux field that peaks just below cloud top (near 1.2 km) and a variation at this level from 22 W m^{-2} at 1300 LST to 98 W m^{-2} at 0400 LST. This cycle of eddy fluxes correlates well with changes in boundary layer moisture, suggesting that the early morning peak in convective activity results in a drying of the subcloud layer due to an enhanced moisture transport out of this layer.
- In general, our observations and computations support the notion that cloud–radiative processes are of primary importance, with large-scale subsidence playing a lesser role in determining the characteristics of the diurnal signal over ASTEX.

Because of the importance of radiative effects in the diurnal variations over ASTEX, one might expect the amplitude of the diurnal cycle to be largest near the time of the summer solstice. This view is supported, in part, by Rozendaal et al. (1995), who observed that the largest diurnal variations in marine low cloudiness as detected in ISCCP data occur during the summer months. This suggests that the diurnal amplitudes observed during the ASTEX period (June 1992) are near their annual maximum.

To provide a larger-scale context for the ASTEX re-

sults summarized above, we also examined the diurnal cycle of low-level divergence over other regions of the North Atlantic. Dai and Deser's diurnal analysis of summertime surface divergence over the North Atlantic (Fig. 16) reveals a complex pattern with alternating phase in latitude belts across the North Atlantic. Diurnal analyses of low-level divergence and vertical motion from three summer field programs (BOMEX, GATE, and ASTEX) support this general picture of alternating phase. The phase difference between the adjacent trade wind and ITCZ regions in the North Atlantic suggests that the Hadley cell over this region pulses diurnally with a stronger circulation in the late morning hours. The relationship between the diurnal cycle of divergent flow in the North Atlantic stratocumulus regime and the diurnally pulsing Hadley cell to its south is unclear and needs further study.

Several mechanisms have been considered to explain the diurnal cycle of low-level winds, divergence, and convection over the North Atlantic. Proposed mechanisms responsible for the diurnal cycle of deep convection over the tropical oceans include the remote response of convection to day–night variations in the tropospheric longwave cooling in clear versus cloudy regions (Gray and Jacobson 1977; Foltz and Gray 1979) and local changes in stability due to direct cloud–radiation interactions (Randall et al. 1991). Radiative and latent heating can also result in diurnally varying forced dynamical responses. Within the trade wind regime of BOMEX, Nitta and Esbensen (1974a) suggested that diurnal variations were a remote response to land–sea heating contrasts from the South American coast. While some evidence exists that a sea-breeze type instability is affecting the BOMEX region, it is far from conclusive. From their global analyses of surface divergence, Dai and Deser (1999) show that a land–sea diurnal circulation exists over many regions of the globe and is likely responsible for the diurnal cycle over oceanic regions close to the continents. The land–sea-breeze mechanism was investigated over the ASTEX domain using a simplified version of a mesoscale model. Preliminary simulations with this model suggest that the land–sea-breeze circulations from the African continent and a larger island in close proximity to PS have little, if any, effect upon the diurnal flow field over ASTEX. However, if we hope to unravel the mechanisms responsible for the complex diurnal flow patterns observed across the North Atlantic, more realistic three-dimensional simulations, including the effects of clouds, radiation, and topography, are required.

Acknowledgments. The authors would like to thank Roger Pielke Sr. and John Strack for running the RAMS simulations to help interpret the diurnal flow features observed over ASTEX. We also wish to thank Nancy Brink for providing hourly buoy data, Shelby Frisch for making available the Porto Santo cloud radar and microwave radiometer data, Richard Taft for his assistance with several of the figures, and Aiguo Dai for allowing us to show his diurnal analysis of summertime surface divergence over the Atlantic. Finally, we thank three anonymous reviewers for their constructive comments, which helped us clarify several key points in this paper. This research was supported by the Office of Naval Research under Grant N00014-91-J-1422 and by NOAA under Grant NA67RJ0152.

APPENDIX

Experimental Design and Model Configuration for Land–Sea Breeze Simulations

The Regional Atmospheric Mesoscale System version 3b (Walko et al. 1995) was used to investigate the effects of sea-breeze circulations from the African continent and Madeira Island on the diurnal flow over the ASTEX domain. Two simulations were run: the first with no offshore island was designed to examine the effects of the African continent alone; the second included an island the approximate size of Madeira (10 km $\times$ 60 km) placed 800 km off the African coast. Both simulations were run on a two-dimensional east–west-oriented grid slice, which was 2000 km in length and 6 km high. The grid was centered at the latitude of Porto Santo (33°N) and at 12°E with a horizontal resolution of 10 km and a variable vertical resolution that ranged from 25 m near the surface to 1000 m near the upper boundary. Simulations were run for 72 h of model time with a time step of 30 s. The Porto Santo mean sounding for June 1992 (Schubert et al. 1992) was used to homogeneously initialize the thermodynamic structure. The kinematic structure was initialized as a state of rest. Land surfaces were assumed to be covered with short grass and topography was ignored. The SST was assigned from a database of mean June values.

In the African simulation with no offshore island, the land–sea-breeze circulation extended offshore ~800 km. In the lowest 3 km, subsidence occurred in the vicinity of PS between 1200 and 2100 LST with a peak subsidence rate of 0.5 cm s^{-1} at 2100 LST. Easterlies winds were observed near PS from 0700 to 1100 LST with westerlies from 1500 to 2300 LST. In the second simulation, which included Madeira, the sea-breeze circulation extended outward about 100 km from the island. In the lowest 3 km, subsidence occurred in the vicinity of PS between 1200 and 1900 LST with a peak subsidence rate of 2.5 cm s^{-1} around 1430 LST. Easterlies winds were observed near PS from 0700 to 2000 LST with westerlies from 2300 to 0500 LST. While certain features in both simulations bear some resemblance to observations at PS (e.g., Figs. 8 and 13 show low-level deviation zonal winds at PS with an easterly component from 0700 to 1300 LST and a westerly component from 1900 to 0400 LST), the simulated vertical motion fields are inconsistent with the diurnal cloud

boundary variations at PS depicted in Fig. 5. The ramifications of these simulations are discussed in the text.

REFERENCES

Albright, M. D., D. R. Mock, E. E. Recker, and R. J. Reed, 1981: A diagnostic study of the diurnal variation in the GATE B-Scale area. *J. Atmos. Sci.,* **38,** 1429–1445.

Augstein, E., H. Riehl, F. Ostapoff, and V. Wagner, 1973: Mass and energy transports in an undisturbed Atlantic trade-wind flow. *Mon. Wea. Rev.*, **101,** 101–111.

Betts, A. K., 1990: Diurnal variation of California coastal stratocumulus from two days of boundary layer soundings. *Tellus,* **42A,** 302–304.

——, C. S. Bretherton, and E. Klinker, 1995: Relation between mean boundary-layer structure and cloudiness at the R/V *Valdivia* during ASTEX. *J. Atmos. Sci.,* **52,** 2752–2762.

Bretherton, C. S., E. Klinker, A. K. Betts, and J. A. Coakley Jr., 1995: Comparison of ceilometer, satellite, and synoptic measurements of boundary-layer cloudiness and the ECMWF diagnostic cloud parameterization scheme during ASTEX. *J. Atmos. Sci.,* **52,** 2736–2751.

Brill, K., and B. A. Albrecht, 1982: Diurnal variations of the trade-wind boundary layer. *Mon. Wea. Rev.,* **110,** 601–613.

Ciesielski, P. E., W. H. Schubert, and R. H. Johnson, 1999: Large-scale heat and moisture budgets over the ASTEX region. *J. Atmos. Sci.,* **56,** 3241–3261.

Cole, H., 1993: The TOGA-COARE ISS radiosonde temperature and humidity sensor errors. NCAR Tech. Rep. SSSF, 26 pp.

Dai, A., and C. Deser, 1999: Diurnal and semidiurnal variations in global surface wind and divergence fields. *J. Geophys. Res.,* **104,** 31 109–31 125.

Delnore, V. E., 1972: Diurnal variation of temperature and energy budget for the oceanic mixed layer during BOMEX. *J. Phys. Oceanogr.,* **2,** 239–247.

Deser, C., and C. A. Smith, 1998: Diurnal and semidiurnal variations of the low-level wind field over the tropical Pacific Ocean. *J. Climate,* **11,** 1730–1748.

Dewart, J. M., 1978: Diurnal variability in the GATE region. Colorado State University, Department of Atmospheric Science Rep. 298, 80 pp.

Duynkerke, P. G., 1989: The diurnal variation of a marine stratocumulus layer: A model sensitivity study. *Mon. Wea. Rev.,* **117,** 1710–1725.

——, and P. Hignett, 1993: Simulation of diurnal variation in a stratocumulus-capped marine boundary layer during FIRE. *Mon. Wea. Rev.,* **121,** 3291–3300.

Fairall, C. W., E. F. Bradley, D. P. Rogers, J. B. Edson, and G. S. Young, 1996: Bulk parameterization of air–sea fluxes for Tropical Ocean-Global Atmosphere Coupled-Ocean Atmosphere Response Experiment. *J. Geophys. Res.,* **101,** 3747–3764.

Foltz, G. S., and W. M. Gray, 1979: Diurnal variation in the troposphere's energy balance. *J. Atmos. Sci.,* **36,** 1450–1466.

Garand, L., C. Grassotti, J. Hallé, and G. L. Klein, 1992: On differences in radiosonde humidity-reporting practices and their implications for numerical weather prediction and remote sensing. *Bull. Amer. Meteor. Soc.,* **73,** 1417–1423.

Gray, W. M., and R. W. Jacobson Jr., 1977: Diurnal variation of deep cumulus convection. *Mon. Wea. Rev.,* **105,** 1171–1188.

Hamming, R. W., 1989: *Digital Filters.* Dover, 284 pp.

Hendon, H. H., and K. Woodberry, 1993: The diurnal cycle of tropical convection. *J. Geophys. Res.,* **98,** 16 623–16 637.

Hignett, P., 1991: Observations of diurnal variation in a cloud-capped marine boundary layer. *J. Atmos. Sci.,* **48,** 1474–1482.

Hogg, D. C., F. O. Guiraud, J. B. Snider, M. T. Decker, and E. R. Westwater, 1983: A steerable dual-channel microwave radiometer for measurement of water vapor and liquid in the troposphere. *J. Climate Appl. Meteor.,* **22,** 789–806.

Holland, J. Z., 1972: Comparative evaluation of some BOMEX measurements of sea surface evaporation, energy flux and stress. *J. Phys. Oceanogr.,* **2,** 476–486.

——, and E. M. Rasmusson, 1973: Measurements of the atmospheric mass, energy, and momentum budgets over a 500-kilometer square of tropical ocean. *Mon. Wea. Rev.,* **101,** 44–55.

Johnson, R. J., P. E. Ciesielski, and K. A. Hart, 1996: Tropical inversions near the 0°C level. *J. Atmos. Sci.,* **53,** 1838–1855.

Lilly, D. K., 1968: Models of cloud-topped mixed layers under a strong inversion. *Quart. J. Roy. Meteor. Soc.,* **94,** 292–309.

Mahrer, Y., and M. Segal, 1985: On the effects of islands' geometry and size on inducing sea breeze circulation. *Mon. Wea. Rev.,* **113,** 170–174.

Martner, B. E., and R. A. Kropfli, 1993: Observations of multi-layered clouds using K_α-band radar. FIRE Cirrus Results, 1993. *Proc. NASA Conf. on FIRE Cirrus Science Results,* Brekinridge, CO, NASA, 75–82.

McBride, J. L., and W. M. Gray, 1980: Mass divergence and vertical velocity in tropical weather systems. Part I: Diurnal variation. *Quart. J. Roy. Meteor. Soc.,* **106,** 501–516.

Miller, M. A., and B. A. Albrecht, 1995: Surface-based observations of mesoscale cumulus-stratocumulus interaction during ASTEX. *J. Atmos. Sci.,* **52,** 2809–2826.

Moyer, K. A., and R. A. Weller, 1997: Observations of surface forcing from the Subduction Experiment: A comparison with global model products and climatological datasets. *J. Climate,* **10,** 2725–2742.

Murakami, M., 1983: Analysis of the deep convective activity over the western Pacific and Southeast Asia. Part I: Diurnal variation. *J. Meteor. Soc. Japan,* **61,** 60–76.

Nicholls, S., 1984: The dynamics of stratocumulus: Aircraft observations and comparisons with a mixed-layer model. *Quart. J. Roy. Meteor. Soc.,* **110,** 783–820.

Nitta, T., and S. Esbensen, 1974a: Diurnal variations in the western Atlantic trades during the BOMEX. *J. Meteor. Soc. Japan,* **52,** 254–257.

——, and ——, 1974b: Heat and moisture budget analyses using BOMEX data. *Mon. Wea. Rev.,* **102,** 17–28.

Orlanski, I., 1973: Trapeze instability as a source of internal gravity waves. Part I. *J. Atmos. Sci.,* **30,** 1007–1016.

Paulson, C. A., E. Leavitt, and R. G. Fleagle, 1972: Air–sea transfer of momentum, heat and water determined from profile measurements during BOMEX. *J. Phys. Oceanogr.,* **2,** 487–497.

Randall, D. A., Harshvardhan, and D. A. Dazlich, 1991: Diurnal variability of the hydrologic cycle in a general circulation model. *J. Atmos. Sci.,* **48,** 40–62.

Reynolds, R. W., 1978: Sea surface temperature anomalies in the North Pacific Ocean. *Tellus,* **30,** 97–103.

Rogers, D. P., X. Yang, P. M. Norris, D. W. Johnson, G. M. Martin, C. A. Friehe, and B. W. Berger, 1995: Diurnal evolution of the cloud-topped marine boundary layer. Part I: Nocturnal stratocumulus development. *J. Atmos. Sci.,* **52,** 2953–2966.

Rotunno, R., 1983: On the linear theory of the land and sea breeze. *J. Atmos. Sci.,* **40,** 1999–2009.

Rozendaal, M. A., C. B. Leovy, and S. A. Klein, 1995: An observational study of diurnal variations of marine stratiform cloud. *J. Climate,* **8,** 1795–1899.

Schubert, W. H., 1976: Experiments with Lilly's cloud-topped mixed layer model. *J. Atmos. Sci.,* **33,** 436–446.

——, S. K. Cox, T. B. McKee, D. A. Randall, P. E. Ciesielski, J. D. Kleist, and E. L. Stevens, 1992: Analysis of sounding data from Porto Santo Island during ASTEX. Colorado State University, Department of Atmospheric Science Rep. 512, 96 pp.

Séze, G., and M. Desbois, 1987: Cloud cover analysis from satellite imagery using spatial and temporal characteristics of the data. *J. Climate Appl. Meteor.,* **26,** 219–249.

Slingo, A., S. Nicholls, and J. Schmetz, 1982: Aircraft observations of marine stratocumulus during JASIN. *Quart. J. Roy. Meteor. Soc.,* **108,** 833–856.

Stevens, E. L., 1994: Comparison of sounding, profiler, radar and ceilometer data from Porto Santo Island during ASTEX. Atmos. Sci. Paper 551, Colorado State University, 72 pp.

Sun, W.-Y., and I. Orlanski, 1981: Large-scale convection and sea breeze circulation. Part I: Stability analysis. *J. Atmos. Sci.,* **38,** 1675–1693.

Wade, C. G., 1995: Calibration and data reduction problems affecting National Weather Service radiosonde humidity measurements. Preprints, *Ninth Symp. on Meteorological Observations and Instrumentation*, Charlotte, NC, Amer. Meteor. Soc., 37–42.

Walko, R. L., W. R. Cotton, M. P. Meyers, and J. Y. Harrington, 1995: New RAMS cloud microphysics parameterization. Part I: The single-moment scheme. *J. Rech. Atmos.,* **38,** 29–62.

Weller, R. A., D. L. Rudnick, R. E. Payne, J. P. Dean, N. J. Pennington, and R. P. Trask, 1990: Measuring near-surface meteorology over the ocean from an array of surface moorings in the subtropical convergence zone. *J. Atmos. Oceanic Technol.,* **7,** 85–103.

White, A. B., C. W. Fairall, and J. B. Snider, 1995: Surface-based remote sensing of the marine boundary-layer cloud properties. *J. Atmos. Sci.,* **52,** 2827–2838.

Yanai, M., S. Esbensen, and J.-H. Chu, 1973: Determination of bulk properties of tropical cloud clusters from large-scale heat and moisture budgets. *J. Atmos. Sci.,* **30,** 611–627.